Journal of Computational Neuroscience, in press.

Systems level circuit model of *C. elegans* undulatory locomotion: mathematical modeling and molecular genetics

Jan Karbowski[1,2,*], Gary Schindelman[1], Christopher J. Cronin[1], Adeline Seah[1], and Paul W. Sternberg[1]

[1] *Howard Hughes Medical Institute and Division of Biology 156-29,*

[2] *Sloan-Swartz Center for Theoretical Neurobiology, Division of Biology 216-76, California Institute of Technology, Pasadena, CA 91125, USA*

Abbreviated title: Circuit model of *C. elegans* locomotion.

Keywords: C. elegans, circuit model for movement, oscillations, mechanosensory feedback, GABA, acetylcholine, calcium, myosin, mutants.

* Corresponding author at: jkarb@its.caltech.edu. Phone: (626)-395-5840.

Abstract

To establish the relationship between locomotory behavior and dynamics of neural circuits in the nematode *C. elegans* we combined molecular and theoretical approaches. In particular, we quantitatively analyzed the motion of *C. elegans* with defective synaptic GABA and acetylcholine transmission, defective muscle calcium signaling, and defective muscles and cuticle structures, and compared the data with our systems level circuit model. The major experimental findings are: (i) anterior-to-posterior gradients of body bending flex for almost all strains both for forward and backward motion, and for neuronal mutants, also analogous weak gradients of undulatory frequency, (ii) existence of some form of neuromuscular (stretch receptor) feedback, (iii) invariance of neuromuscular wavelength, (iv) biphasic dependence of frequency on synaptic signaling, and (v) decrease of frequency with increase of the muscle time constant. Based on (i) we hypothesize that the Central Pattern Generator (CPG) is located in the head both for forward and backward motion. Points (i) and (ii) are the starting assumptions for our theoretical model, whose dynamical patterns are qualitatively insensitive to the details of the CPG design if stretch receptor feedback is sufficiently strong and slow. The model reveals that stretch receptor coupling in the body wall is critical for generation of the neuromuscular wave. Our model agrees with our behavioral data (iii), (iv), and (v), and with other pertinent published data, e.g., that frequency is an increasing function of muscle gap-junction coupling.

Introduction

Caenorhabditis elegans nematode worms, with a small nervous system comprising only 302 neurons (White et al, 1986), move by generating an oscillatory neuromuscular wave that alternates dorsal and ventral muscles (Brenner, 1974; Chalfie et al, 1985; Karbowski et al, 2006). The molecular, cellular, and network mechanisms of this oscillatory spatio-temporal activity are virtually unknown. Their understanding may provide insight about the relationship between neuromuscular dynamics and how behavior is created in these extensively genetically studied animals (Bargmann, 1998; Hobert, 2003; de Bono and Maricq, 2005; Gray et al, 2005), and might be potentially relevant for other locomotory systems. It has proven difficult to address these questions using standard electrophysiological techniques in *C. elegans* because of its small neural sizes (Francis et al, 2003). In this paper, we use a combination of genetic perturbations, behavioral assays combined with a quantitative tracking system, and mathematical modeling to decipher dynamical properties of a detailed neuromuscular circuit relevant for *C. elegans* movement. By combining these approaches and building a mathematical circuit model we seek to bridge the gap between molecular/cellular and systems level understandings of undulatory locomotion (Fig. 1).

We investigate specific questions related to the mechanisms that control body undulations and coordination: (i) How do different elements in the *C. elegans* neuromuscular circuit interact to produce both body oscillations and neuromuscular wave? In particular, where is the primary oscillatory signal generated? (ii) How does mechanosensory feedback (stretch receptor coupling) affect locomotion? Does it play any role in

generating a neuromuscular wave? If so, how does its strength affect the wavelength (intermuscle phase lag) of muscle contractions? (iii) How does synaptic coupling between neurons affect locomotory rhythm? Is there any qualitative difference between excitation and inhibition on oscillatory frequency? Are there optimal values for the synaptic couplings? (iv) How does gap-junction coupling between body-wall muscles and structural defects in muscles and cuticle affect movement?

To address these questions we employed a parallel approach of collecting experimental data and making model predictions in an iterative manner. In particular, we quantitatively analyzed the motion of different neuronal and non-neuronal mutants by measuring their kinematic parameters (Fig. 1B) and relating them to the dynamic properties of our circuit model. Investigated mutants included worms with decreased and increased synaptic GABA transmission, altered acetylcholine transmission, altered levels of calcium signaling in muscles, and worms with structural defects in muscles (myosin) and cuticle.

Materials and Methods

Experimental part

Description of analyzed mutants. We examined the locomotion of several *C. elegans* mutants with affected inhibitory synaptic transmission (GABA), excitatory synaptic transmission (acetylcholine), and muscular function (calcium channels and myosin). We investigated mutants with both decreased and increased GABA function. For mutations effectively decreasing inhibition we studied: *unc-25(e156)*, which encodes glutamic acid decarboxylase (GAD) - the biosynthetic enzyme for GABA production (Jin et al, 1999); *unc-46(e177)* (*him-5(e1490)* was in the background), which presumably plays a modulatory role in GABA packaging into vesicles (Schuske et al, 2004); and *unc-18(e81)* mutants carrying the *syEx995[cho-1::unc-18::yfp]* transgene. *unc-18* functions as a facilitator of vesicles docking at presynaptic neurons (Weimer et al, 2003) and is expressed in both cholinergic and GABAergic neurons (Gengyo-Ando et al, 1993). Therefore, in the *unc-18(e81)* strain carrying *syEx995[cho-1::unc-18::yfp]* we have restored *unc-18* function specifically to cholinergic neurons using the *cho-1* promoter (Okuda et al, 2000), leaving the GABAergic neurons non-functional. For a mutation effectively increasing inhibition we studied *slo-1(js118)* mutants with extrachromosomal *Pacr-2::slo-1(+)* transgene. SLO-1 encodes a Ca^{2+} activated K^{+} channel that presumably counteracts quantal synaptic neurotransmission both in excitatory and inhibitory neurons (Wang et al, 2001), and removal of this channel (in *slo-1* mutants) leads to an increased neurotransmission above wild-type level. *slo-1(js118)* worms with

the *Pacr-2::slo-1(+)* transgenes (syEx996, syEx988, and syEx991) have elevated neurotransmitter release in inhibitory neurons, but they have restored wild-type release levels in excitatory neurons because *Pacr-2::slo-1(+)* drives expression of wild-type *slo-1* in these neurons (Davies et al, 2003). We also studied three types of strains with presumably elevated acetylcholine (excitatory) synaptic signaling and wild-type level of GABA: *slo-1(js118); Punc-25::slo-1*, *slo-1(js118); Punc-17::slo-1*, and *slo-1(js118); Pcho-1::slo-1*.

For mutations affecting muscular calcium function, we studied *unc-68* mutants, as well as *egl-19(n582)* rescued with an *unc-119::egl-19::yfp* transgene. *unc-68* gene encodes ryanodine receptor channels that gate the release of calcium ions from internal stores in both body-wall muscle cells and in pharyngeal muscle (Maryon et al, 1996; Maryon et al, 1998). We analyzed the locomotion of loss-of-function *unc-68(r1158)* worms, which exhibit incomplete flaccid paralysis. The *egl-19* gene plays an important role in regulating muscle excitation and encodes the $\alpha 1$ subunit of a homologue of vertebrate L-type voltage-activated Ca^{2+} channels (Lee et al, 1997). Similarly, we analyzed the locomotion of *egl(n582)* mutants carrying an *unc-119::egl-19::yfp* transgene, which restores *egl-19* function specifically in neurons using the *unc-119* promoter to drive pan-neuronal expression of *egl-19* (Maduro and Pilgrim, 1995). This partial loss-of-function strain have slow muscle depolarization and feeble contractions (Lee et al, 1997; Jospin et al, 2002).

For mutations affecting muscle and cuticle structure we analyzed *unc-54*, *sqt-1*, and BE109 worms. *unc-54* worms carry mutations in the head region of body-wall

muscle myosin. We analyzed the following strains: RW130 *unc-54(st130)*, RW132 *unc-54(st132)*, RW134 *unc-54(st134)*, RW135 *unc-54(st135)*, RW5008 *unc-54(s95)*, and BC347 *unc-54(s74)*. These mutations are hypothesized to alter the contraction-relaxation cycle of the myosin-actin crossbridge formation by increasing its duration (Moerman and Fire, 1997). *sqt-1* gene encodes cuticle collagen and we analyzed two strains: BE101 *sqt-1(sc101)* and BE103 *sqt-1(sc103)*. BE109 mutants have defective cuticle struts (J. Kramer, pers. communication).

Construction of plasmids and strains is described in the Supplementary Information.

Locomotory data extraction and processing. We video recorded and digitized the motion of young adult hermaphrodite worms (mutants and wild-type) 15-20 hr post mid-L4 developmental stage on an agar plate with thin film of *E. coli* OP50 bacteria and LB media. The video recording and data extraction was done using a device specially designed for studying *Caenorhabditis* locomotion (Cronin et al, 2005). We collected 5 minutes of video per worm, extracting digital locomotion data from the middle 4 minutes. Such 4 minute windows average over many possible sensory influences that can vary among worms and thus statistically minimize the variability of external conditions. From these data we derived distributions of the undulatory frequency and bending flex by dividing worm's body into 12 sections which served as worm's system of coordinates. Local flex angle was determined as described in Fig. 1B. To derive the bending frequencies for each articulation point we first calculate a time-ordered matrix of angles between each pair of adjacent body sections (that is, at each articulation point). Next we apply Mat-

lab's spectrogram function (specgram) to the vector of changing bend angles at each articulation point, which yields a time-ordered matrix of the relative energies of the changing bend angles' component frequencies. The highest magnitude, non-constant component frequency from each time window is that window's characteristic bending frequency. Frequencies and flexes for each articulation point in Figs. 3-6 are population averages. In Figs. 5 and 6 we used non-parametric sign test for paired samples to determine if average frequencies between different mutants are significantly different.

Theoretical part

Circuit model. All known locomotory systems use some form of a Central Pattern Generator (CPG) circuit to generate rhythm (Grillner, 1975; Delcomyn, 1980; Marder and Calabrese, 1996; Nusbaum and Beenhakker, 2002). Mechanosensory feedback usually alters the rhythm; however, its importance varies in different animals and even in the same animal under different conditions (Marder et al, 2005). At one extreme, it can play a minor modulatory role (Grillner, 1975; Delcomyn, 1980), at the other, it can be critical for body coordination (Friesen and Cang, 2001; Akay et al, 2004).

The global circuit responsible for *C. elegans* forward locomotion is constructed based on neuroanatomical data (Chalfie et al, 1985; White et al, 1986). It is composed of the head and body wall neural networks (Fig. 2A,B) connected partly via two interneurons AVB and PVC, which are implicated as controllers of forward movement (Chalfie et al, 1985), and partly via muscle gap junctions. AVB and PVC receive massive synaptic input from the head neurons and target only excitatory motor neurons (type B neurons:

ventral VB and dorsal DB) in the body wall (White et al, 1986). AVB connects them via gap junctions and PVC via chemical synapses. We assume, following theoretical predictions (Wicks et al, 1996), that the latter synapses are excitatory.

The real head neural network is composed of about 200 neurons with mostly unknown polarities and complicated wiring diagram (White el al, 1986). Inclusion of all of these elements in our circuit model would increase its complexity (the number of parameters) by at least an order of magnitude, which would obscure the basic mechanisms. Instead, we decided to depict the head network in a simplified manner with lesser but essential number of elements. This simplified approach has an advantage of being conceptually comprehensible. Thus our head neural network is comprised of head interneurons and ventral and dorsal head motor neurons (Fig. 2B). The head motor neurons contain both excitatory neurons (White et al, 1986) and a pair of GABA-ergic inhibitory RME neurons (Schuske et al, 2004). Because connectivity patterns between actual head interneurons form numerous feedback loops (e.g., AIZ $\rightarrow$ AIA $\leftrightarrow$ AWA $\rightarrow$ AIZ and RIB $\leftrightarrow$ RIG $\leftrightarrow$ URY $\rightarrow$ RIB; see White et al, 1986), we mimicked this phenomenon by two (dorsal and ventral) interneuron loops X$\rightarrow$ Y$\rightarrow$ Z$\rightarrow$ X. These loops can in principle generate a primary rhythm in the head, which is then imposed on downstream networks along the body via muscle coupling and/or AVB and PVC interneurons. The loop X, Y, Z is the minimal circuit in the *C. elegans* head interneurons that can generate robust oscillations. We include mechanosensory feedback in our head network model following suggestions that a pair of head interneurons SAA may contain stretch receptors on their long dendrites (White et al, 1986).

The body wall forward motion network (White et al, 1986) is composed of ventral and dorsal sub-circuits that contain motor neurons, body wall longitudinal muscles, and feedback loops associated with mechanosensation (Fig. 2A). The neuronal part of each sub-circuit consists of several cholinergic excitatory B motor neurons (ventral VB and dorsal DB), and several GABA-ergic inhibitory motor neurons (type D neurons: ventral VD and dorsal DD) (Chalfie et al, 1985; McIntire et al, 1993; Schuske et al, 2004). Apart from gap junctions from AVB and chemical synapses from PVC, the excitatory B neurons receive synaptic input from DVA interneuron (DVA synapses on some B neurons, see White et al, 1986). Anatomically, the role of this interneuron in locomotion is not clear, and it was suggested (Li et al, 2006) that it might serve as a neuromodulator involved in detecting body stretch, with no definite synaptic polarity. We assume that the overall influence of this neuron is inhibitory. This inhibitory input is necessary to prevent spontaneous oscillations in the body-wall circuit when it is disconnected from the head. Coupling between ventral and dorsal motor sub-circuits is mediated partly via excitatory synapses terminating on inhibitory D motor neurons of the complementary circuit (Fig. 2A), and partly via AVB gap-junctions. An effective cross-inhibition (B $\rightarrow$ D) between the two sub-circuits amplifies their alternating oscillatory activities (Fig. 2A, and below). Neighboring motor neurons, as well as neighboring muscles are connected via gap junctions (D. Hall, pers. commun). Mechanosensory feedback in the body wall, similarly as in the head, is associated with hypothetical stretch receptors. Following the Byerly and Russell hypothesis (in Chalfie and White, 1988), we assume that stretch receptors are located on the extended dendritic processes of the excitatory

B motor neurons (VB and DB). In the forward motion circuit, all these dendrites are directed posteriorly. We assume that mechanosensors transduce local body stretch along excitatory motor neuron dendrites to the somas of these neurons by polarizing them, since mechano-stimulation is known to increase cell excitability (Goodman and Schwarz, 2003). Thus, mechanosensory feedback coupling along the body wall is non-local, excitatory, and unidirectional in nature.

The theoretical part of this study deals almost exclusively with forward motion, which is a dominant behavior in *C. elegans*. Backward motion is considered only briefly in the context of neuromuscular wave directionality (see below). The backward motion is controlled by a complementary system of 3 interneurons (AVA, AVD, AVE) and type A excitatory motor neurons (ventral VA and dorsal DA). The latter neurons have long dendrites directed anteriorly, i.e., opposite to the corresponding motor neurons in the forward motion circuit (Chalfie et al, 1985). The behavioral transitions between forward and backward motion will be addressed in a future study.

Equations used in the theoretical model. We assume that the activities of motor neurons are graded, since experimental data show the absence of action potentials in the sensory neuron ASER (Goodman et al, 1998), which is consistent with the lack of voltage-activated sodium channels in the *C. elegans* genome (Bargmann, 1998). Additional support for this assumption comes from neurophysiological recordings in a related, larger, nematode *Ascaris*, which has a similar nervous system, and lacks action potentials in all recorded neurons (Davis and Stretton, 1989). Below we provide

equations governing activities of all neurons, muscles, and stretch receptors included in the model. These equations were solved on a Linux-system computer using a standard second-order Runge-Kutta method in Fortran (F77).

The dynamics of head interneurons controlling the ventral side of the head are represented by:

$$\tau_x \frac{dX_v}{dt} = -X_v + c_1 + w_{xs}\mathbf{H_{xs}}(S_{hv}) - w_{xz}\mathbf{H_{xz}}(Z_v) - w_{xi}\mathbf{H_{xi}}(I_{hv}) + g_{avb}(V_{avb} - X_v), \quad (1)$$

$$\tau_y \frac{dY_v}{dt} = -Y_v + w_{yx}\mathbf{H_{yx}}(X_v) + g_{avb}(V_{avb} - Y_v), \quad (2)$$

$$\tau_z \frac{dZ_v}{dt} = -Z_v + w_{zy}\mathbf{H_{zy}}(Y_v) + w_{zx}\mathbf{H_{zx}}(X_d) + g_{avb}(V_{avb} - Z_v), \quad (3)$$

where X_v and Y_v denote the activities of two excitatory ventral head interneurons, X_d denotes the activity of a corresponding head dorsal interneuron, Z_v is the activity of ventral inhibitory interneuron, and τ_x, τ_y, τ_z are corresponding time constants. S_{hv} is the head stretch receptor activity situated on the ventral interneuron X_v, and I_{hv} is the membrane potential of head inhibitory ventral motor neuron. V_{avb} is the membrane potential of AVB interneuron and g_{avb} is the gap junction strength between AVB and X, Y, and Z. The parameter c_1 denotes some input coming from other head neurons and it can be either excitatory (positive) or inhibitory (negative), depending on the worm's "internal state". The parameters $w_{\alpha\beta}$ characterize the strength of chemical synapses

between circuit elements from β to α, and most of the genetic mutations we examined affect precisely these parameters. The functions $\mathbf{H}_{\alpha\beta}$ are positively defined sigmoidal functions of the form: $\mathbf{H}_{\alpha\beta}(x) = (1 + \tanh[(x - \theta_{\alpha\beta})/\eta_{\alpha\beta}])$, where $\theta_{\alpha\beta}$ is the threshold for activation and $\eta_{\alpha\beta}$ characterizes the steepness of the nonlinearity. The equations for the dorsal side of the head are analogous with a subscript substitution $v \leftrightarrow d$.

The dynamics of the ventral side head motor neurons, muscles, and stretch receptor feedback are given by:

$$\tau_e \frac{dE_{hv}}{dt} = -E_{hv} + w_{ey}\mathbf{H_{ey}}(Y_v), \tag{4}$$

$$\tau_i \frac{dI_{hv}}{dt} = -I_{hv} + w_{ie}\mathbf{H_{ie}}(E_{hv}), \tag{5}$$

$$\begin{aligned}\tau_m \frac{dM_{hv}}{dt} = &-M_{hv} + w_{mm}\mathbf{H_{mm}}(M_{hv}) + \tilde{w}_{me}\mathbf{H_{me}}(E_{hv}) \\ &-\tilde{w}_{mi}\mathbf{H_{mi}}(I_{hd}) + g_m(M_{v,1} - M_{hv}),\end{aligned} \tag{6}$$

$$\tau_s \frac{dS_{hv}}{dt} = -S_{hv} + w_{sm}\left[\mathbf{H_{sm}}(M_{hd} - M_{hv}) - 1\right], \tag{7}$$

where E_{hv} and I_{hd} are the membrane potentials of head ventral excitatory and dorsal inhibitory motor neurons respectively, M_{hv} and M_{hd} are head ventral and dorsal muscle membrane potentials, and τ_e, τ_i, τ_m, τ_s are their respective time constants. The steady-state value of the stretch receptor activity S_{hv} should be proportional to the degree of head bending, which we assume is a sigmoidal function of the differences in

ventral and dorsal muscle activities. Note that stretch receptors are activated if there is initial asymmetry in activities of ventral and dorsal muscles. Apart from synaptic input, a muscle cell is also activated by a voltage-activated calcium channels, which in the model is represented by a self-promoting $\mathbf{H_{mm}}(M_{hv})$ term with the coupling w_{mm} characterizing the calcium signaling strength. Identical equations describing the dorsal side are obtained with a subscript substitution $hv \leftrightarrow hd$.

The dynamics of the two forward motion interneurons AVB and PVC are given by:

$$\begin{aligned}\tau_{avb}\frac{dV_{avb}}{dt} = &-V_{avb} + w_{avb,x}\left[\mathbf{H_{avb,x}}(X_v + Y_v) + \mathbf{H_{avb,x}}(X_d + Y_d)\right] \\ &+w_{avb,pvc}\mathbf{H_{avb,pvc}}(V_{pvc}) + g_{avb,e}\sum_{i=1}^{N}\left(E_{v,i} + E_{d,i} - 2V_{avb}\right) \\ &+g_{avb}\left(X_v + Y_v + Z_v + X_d + Y_d + Z_d - 6V_{avb}\right), \end{aligned} \tag{8}$$

$$\tau_{pvc}\frac{dV_{pvc}}{dt} = -V_{pvc} + w_{pvc,x}\left[\mathbf{H_{pvc,x}}(X_v + Y_v) + \mathbf{H_{pvc,x}}(X_d + Y_d)\right], \tag{9}$$

where V_{avb} and V_{pvc} are the membrane potentials of AVB and PVC interneurons and τ_{avb}, τ_{pvc} are their respective time constants. $E_{v,i}$ and $E_{d,i}$ denote the membrane potentials of the ith ventral (VB type) and dorsal (DB type) excitatory motor neurons, respectively. The parameter $g_{avb,e}$ is the gap-junction coupling between AVB and the body wall excitatory motor neurons. N denotes the numbers of excitatory and inhibitory motor neurons on both sides of the body wall; in simulations we take $N = 8$.

The ventral side of the body wall nervous system is represented by a set of equations:

$$\tau_e \frac{dE_{v,i}}{dt} = -E_{v,i} + c_2 + w_{e,pvc}\mathbf{H_{e,pvc}}(V_{pvc}) + w_{es}\mathbf{H_{es}}(S_{v,i+1}) + g_{avb,e}(V_{avb} - E_{v,i}) + g_e\left(E_{v,i+1} + E_{v,i-1} - 2E_{v,i}\right), \tag{10}$$

$$\tau_i \frac{dI_{v,i}}{dt} = -I_{v,i} + w_{ie}\mathbf{H_{ie}}(E_{d,i}) + g_i\left(I_{v,i+1} + I_{v,i-1} - 2I_{v,i}\right), \tag{11}$$

$$\tau_m \frac{dM_{v,i}}{dt} = -M_{v,i} + w_{mm}\mathbf{H_{mm}}(M_{v,i}) + w_{me}\mathbf{H_{me}}(E_{v,i}) - w_{mi}\mathbf{H_{mi}}(I_{v,i}) + g_m\left(M_{v,i+1} + M_{v,i-1} - 2M_{v,i}\right), \tag{12}$$

$$\tau_s \frac{dS_{v,i}}{dt} = -S_{v,i} + w_{sm}\left[\mathbf{H_{sm}}(M_{d,i} - M_{v,i}) - 1\right], \tag{13}$$

where $I_{v,i}$ is the membrane potential of the ith ventral inhibitory motor neuron (VD type), and $S_{v,i}$ is the stretch receptor activity related, as in the head, to the relative activities of the ventral $M_{v,i}$ and dorsal $M_{d,i}$ muscles. By the nature of connectivity in our network, $M_{v,0} \equiv M_{hv}$ and $M_{d,0} \equiv M_{hd}$. Note that the ith excitatory motor neuron $E_{v,i}$ (corresponding to VB type) is affected by the stretch receptors at $(i+1)$th position in the forward motion circuit. (In the backward motion circuit $E_{v,i}$ corresponds to VA neuron and is affected by the stretch receptor at $(i-1)$th position.) The parameters g_e, g_i, and g_m are the gap-junction couplings among excitatory motor neurons, inhibitory motor neurons, and among muscles, respectively. The parameter c_2 denotes inhibition coming to the excitatory motor neurons (VB, DB) from the DVA interneuron, and its negative value prevents spontaneuos oscillations in the body wall circuit when it

is disconnected from the head circuit. These spontaneous oscillations emerge because of the numerous closed loops in the body wall, which contains both excitatory and inhibitory elements (VB $\rightarrow$ DD $\rightarrow$ M_d $\rightarrow$ S_d $\rightarrow$ DB $\rightarrow$ VD $\rightarrow$ M_v $\rightarrow$ S_v $\rightarrow$ VB), see Fig. 2A. Identical equations describe a dorsal part of the body wall circuit, with a substitution $v \leftrightarrow d$. The ventral inhibitory motor neuron $I_{v,i}$ (VD type) is activated by the activity of the dorsal excitatory motor neuron $E_{d,i}$ (DB type).

In simulations we rescale uniformly almost all synapses both in the head and in the body wall by two factors: q_{ex} corresponding to excitatory synapses, and q_{in} corresponding to inhibitory GABA synapses. Both parameters are variable and characterize global levels of excitation and inhibition, respectively. The values of parameters used in simulations are presented in Table 1. Values of these parameters were chosen arbitrarily and a global circuit function (i.e. sustained oscillations), to a large extent, does not depend on their precise values. Oscillations in the circuit emerge for c_1 between 0.5 and 2.5. Models A and B differ only in one aspect, i.e., the degree of nonlinearity in interactions (in functions $\mathbf{H}$) between head interneurons X, Y, Z. Model A was obtained by taking the corresponding steepness parameters η to be small (high nonlinearity), whereas model B was obtained by increasing values of these parameters (low nonlinearity). The rest of the parameters are the same for both models. In all theoretical figures we used the parameters from Table 1, unless indicated otherwise.

The Fortran code for simulating of Eqs. (1)-(13) will be deposited in *ModelDB* database.

Results

To begin an analysis of how the circuit controls locomotion, we chose specific genetic perturbations that affect easily identifiable classes of parameters in the neuroanatomical circuit. These parameters can be manipulated in our theoretical model, enabling a comparison between theory and experiment.

Experimental results

The major experimental findings detailed below are: (i) anterior-to-posterior spatial gradients of flex angle for almost all strains, and for neuronal mutants, also analogous weak gradients of frequency, both for forward and backward motion, (ii) cuticle and muscle (non-neuronal) mutants affect locomotion characteristics, suggesting the existence of some form of mechanosensory feedback, (iii) invariance of wavelength characterizing the neuromuscular wave, (iv) biphasic dependence of undulatory frequency on synaptic GABA signaling, and a plausible biphasic dependence on acetylcholine signaling, and (v) strong decrease of undulatory frequency with increasing muscle time constant characterizing the cycle of myosin-actin crossbridge formation.

Spatial distribution of undulatory frequency and bending flex. The spatial distribution of some locomotory parameters may provide clues about how the motion is generated and coordinated in *C. elegans* worms. We measured frequency of undulations and bending flex, defined as a maximal local bending angle of worm's body, as a function of their distance from the head. The frequency for wild-type and most non-neuronal

mutants is either constant or nearly constant both for forward and backward motion (Fig. 3A,B, and Supplementary Table T1), with the exception of *sqt-1* (lacking one cuticle collagen), for which the frequency decreases significantly toward the tail (e.g., in *sqt-1(sc103)*, the head and tail oscillate at respectively 0.29 ± 0.07 Hz and 0.22 ± 0.09 Hz in forward motion, and corresponding values in backward motion are: 0.22 ± 0.05 Hz and 0.12 ± 0.04 Hz; see Suppl. Table T1). In contrast, all neuronal mutants display a monotonic decay of the frequency directed posteriorly, in some cases up to 50 % (see Suppl. Table T1). Specifically, we obtained the following frequencies in the head and tail for neuronal mutants. For *unc-25(e156)*: 0.36 ± 0.07 Hz in the head and 0.23 ± 0.06 Hz in the tail (forward motion), and 0.20 ± 0.08 Hz in the head and 0.13 ± 0.03 Hz in the tail (backward motion); for *unc-46(e177)*: 0.29 ± 0.03 Hz in the head and 0.16 ± 0.07 Hz in the tail (forward motion), and 0.26 ± 0.02 Hz in the head and 0.13 ± 0.04 Hz in the tail (backward motion); for *unc-18(e81); cho-1::unc-18:yfp*: 0.20 ± 0.08 Hz in the head and 0.09 ± 0.04 Hz in the tail (forward motion), and 0.16 ± 0.05 Hz in the head and 0.06 ± 0.02 Hz in the tail (backward motion); for *slo-1(js118)*: 0.38 ± 0.07 Hz in the head and 0.29 ± 0.08 Hz in the tail (forward motion), and 0.32 ± 0.07 Hz in the head and 0.16 ± 0.06 Hz in the tail (backward motion). These data indicate that for neuronal mutants tail oscillations have substantially smaller frequencies than head oscillations.

The behavior of the flex is more universal (Fig. 3C,D and Suppl. Table T1). For almost all mutants and wild-type worms, and for both forward and backward motion, there is a pronounced decay of the flex from the head up to some point close to the tail. From that point the flex either stays constant or slightly increases towards the tail.

Overall, the flex and position exhibit statistically significant strong negative correlations (Fig. 3 C,D). Thus, surprisingly, the opposite motions yield similarly directed anterior-to-posterior gradients of the flex.

Some non-neuronal mutants dramatically alter frequency. We find that it is relatively easy to change the undulatory frequency of worms by genetically modifying some of non-neuronal parameters. As an example, mutants with affected cuticle function (collagen defective *sqt-1* mutants or strut defective BE109 mutants) and mutants with altered muscle function (myosin defective *unc-54* mutants) exhibit different locomotory outputs than the wild-type worms, with substantially reduced frequency (Fig. 4). Also, results (see below) on mutants with defects in muscle calcium signaling (*unc-68*) show that their frequency is significantly lower than wild-type. The fact that non-neuronal mutants have profoundly altered locomotory parameters, in particular frequency and flex, indicates that there must be some feedback coupling between the nervous system of *C. elegans* and its muscular and cutico-skeletal systems.

Conservation of wavelength. We measured the wavelength of neuromuscular wave in wild type and several mutants (Table 2). The ratio of the wavelength to the actual worm's body length is relatively constant across different worms and appears to be identical for forward and backward motion. Since these worms move with different frequencies, the data in Table 2 suggest that wavelength is essentially frequency independent.

Biphasic dependence of undulatory frequency on GABA (inhibitory) transmission. We analyzed the motion of mutants defective in GABA function primarily in the ventral cord motor neurons. All three uncoordinated neuronal mutants - *unc-25(e156)*, *unc-46(e177)*, and *unc-18(e81)* rescued with transgene *syEx981[cho-1::unc-18::yfp]* in cholinergic neurons - have decreased GABA transmission as compared to wild type (McIntire et al, 1993; Weimer et al, 2003). These animals have also much lower frequencies of undulations than wild-type worms (Fig. 5A and Suppl. Table T1, $p < 0.05$).

We also studied the behavior of worms with increased GABA transmission. Since no known mutants have this property exclusively, we constructed and analyzed several transgenic strains with altered GABAergic and cholinergic signaling based on *slo-1(js118)* mutation, which elevates globally both types of neurotransmission by eliminating a particular calcium activated potassium channel (Wang et al, 2001) (Suppl. Table T2). By using different promoters we constructed worms that restore either excitation or inhibition to normal levels by making K^+ channel functional in either cholinergic or GABA-ergic neurons. The *slo-1(js118); Pacr-2::slo-1* worms have presumably rescued cholinergic transmission to the wild-type level, but GABA transmission is still elevated. These worms are significantly slower ($p < 0.05$) than wild-type worms (Fig. 5B). For consistency, we also compared *slo-1(js118); Pacr-2::slo-1* animals to two strains with presumably wild-type levels of both GABA and acetylcholine, i.e., *slo-1(js118); Pacr-2::slo-1; Punc-25::slo-1* and *slo-1(js118); Psnb-1::slo-1* (Fig. 5C). In this case *slo-1(js118); Pacr-2::slo-1* are also significantly slower ($p < 0.05$). Thus, the behavior of worms with increased GABA signaling (Figs. 5B,C) is qualitatively similar to the

behavior of worms with decreased GABA (Fig. 5A): the undulatory frequency of worms with altered GABA transmission, either below or above the wild-type level, is always smaller than wild type.

To summarize, all these results clearly suggest a non-monotonic (biphasic) dependence of the undulatory frequency on the inhibitory synaptic GABA signaling in the worm.

Dependence of undulatory frequency on acetylcholine (excitatory) transmission. Various constructs with *slo-1* enable us to determine the dependence of frequency on excitatory coupling in *C. elegans* (Suppl. Table T2). *slo-1(js118); Pacr-2::slo-1* animals with presumably rescued levels of acetylcholine transmission to the wild-type level but elevated GABA transmission are either slightly faster or slightly slower than the control *slo-1(js118); Pacr-2::gfp* with both increased GABA and increased acetylcholine signaling (Fig. 6A). Thus, a decrease of excitatory transmission does not lead to a clear-cut phenotype, which might suggest a possible non-monotonic dependence of the frequency on a global synaptic excitation. In the case of worms with increased acetylcholine signaling and presumably wild-type level of GABA (three strains: *slo-1(js118); Punc-25::slo-1*, and *slo-1(js118); Punc-17::slo-1*, and *slo-1(js118); Pcho-1::slo-1*), we observe their slightly lower frequencies than wild type (Fig. 6B). This case, in turn, suggests that increasing global excitation leads to a slight decrease in undulatory frequency (see, however, "Comparison of the theory with the experimental data" section below).

Frequency decreases sharply with increasing muscle time constant. Fig. 3 and Supple-

mental Table T1 show that all strains of *unc-54* mutants move with frequencies much lower than wild type. These mutants have affected muscle myosin in the body wall, which presumably increases the time constant controlling contraction-relaxation cycle of myosin-actin crossbridge. Thus, increase in muscle time constant leads to a pronounced decrease in the undulatory frequency both for forward and backward motion.

Dependence of undulatory frequency on muscle calcium signaling. We studied locomotion of *C. elegans* mutants with defective calcium signaling in body wall muscle cells. Null *unc-68* mutants, which have defective ryanodine receptor channels responsible for release of stored calcium ions, display abnormal locomotion (Maryon et al, 1996; Maryon et al, 1998). We analyzed the motion of loss-of-function *unc-68(r1158)* worms with reduced levels of calcium in muscles, and found that their frequencies of undulations are smaller than that of the wild-type worms (Suppl. Table T1 and Fig. S1), in agreement with Maryon et al. (1996, 1998).

We also analyzed locomotion of loss-of-function *egl-19(n582)* animals carrying a transgene expressing EGL-19-YFP in neurons (*unc-119::egl-19::yfp*). This strain has a defective voltage-gated Ca^{+2} channel in body wall muscles but has its function restored in neurons. These worms have less muscle calcium influx (Jospin et al, 2002) and lower frequency of undulations than wild type (Suppl. Table T1 and Fig. S1), similarly to the *unc-68* worms.

These data suggest that decreasing calcium signaling in muscle cells leads to decrease in the frequency of body oscillations. Moreover, because *unc-68* is expressed almost exclusively in muscles (Maryon et al, 1998), and *egl-19(n582); unc-119::egl-19::yfp* has a

defect also only in muscles, these results provide an additional support for our hypothesis about the existence of a feedback coupling between body wall muscles and the neural circuits.

Theoretical results

The major theoretical findings detailed below are: (i) the dynamic properties of the global circuit practically do not depend on CPG design in the head if stretch receptor feedback is sufficiently strong and slow, (ii) the neuromuscular wave is generated due to a nonlocal stretch receptor feedback coupling in the body wall, and its wavelength is almost frequency and stretch receptor coupling (if strong enough) independent, (iii) the frequency of oscillations depends in a biphasic manner on both inhibitory and excitatory synaptic coupling, (iv) the frequency increases monotonically with muscle gap-junction coupling strength, and (v) the frequency decreases with increasing time constants of the circuit elements. We also predict that frequency should depend non-monotonically on muscle calcium signaling. We made no attempt to fit quantitatively the experimental data, since many physiological parameters in *C. elegans* are unknown. In this sense, our approach is qualitative. However, we adjusted model parameters, especially τ_s, to obtain frequencies of the same order of magnitude as in experiments.

Oscillation generation. We assume that primary oscillations necessary for a regular movement (i.e., spontaneous and not caused by an outside mechanical stimulation) are generated in the head. The arguments, based on the anterior-to-posterior gradient

of the flex (Fig. 3), supporting the head as a likely primary CPG are presented in the Discussion. We consider two extreme design versions of the head CPG. In model A, the stretch receptor feedback plays a minor modulatory role in affecting neurally generated rhythm (neural component dominates). On the other hand, in model B, the stretch receptor feedback plays a critical role in rhythm generation (reflex component dominates). In model A oscillations are generated in the head interneuron circuit, i.e., in the loop X $\rightarrow$ Y $\rightarrow$ Z $\rightarrow$ X, provided nonlinearities in the interactions between these interneurons are sufficiently strong (corresponding sigmoidal functions $\mathbf{H}_{\alpha\beta}$ have sharp thresholds for activation). The emerging oscillatory patterns are presented in Fig. 7A,C. One of the roles of the stretch receptor feedback in model A is to slow down the emerging rhythm as compared to a purely neural oscillator by introducing temporal delays. (This is because the characteristic membrane time constant of *C. elegans* neurons should be of the order of 100 msec, as it is in morphologically similar *Ascaris* neurons (Davis and Stretton, 1989) and much larger mammalian neurons. As a result, a purely neural rhythm would give $\sim$ 10 Hz body undulations, which is 20-30 times larger than that observed experimentally; Suppl. Table T1.) In model B, the primary oscillations in the head are generated because of the presence of the stretch receptor feedback and its interaction with neurons, i.e. in the loop X $\rightarrow$ Y $\rightarrow$ E $\rightarrow$ M $\rightarrow$ S $\rightarrow$ X. Oscillations in this model are generated even when the interneuron circuit (X, Y, Z) is intrinsically non-oscillatory, i.e., when interactions between interneurons are only weakly nonlinear or linear. In this case, however, the prerequisite for the appearance of oscillations is initial asymmetry in activities between ventral and dorsal sides, which

is necessary for engaging the stretch receptor feedback. Such activity asymmetry can be facilitated by nonequal number of dorsal and ventral motor neurons present in *C. elegans*. The emerging oscillatory patterns in model B are presented in Fig. 7B,D.

In both models of CPG, the crucial element for oscillation generation is a net nonlinear negative feedback loop destabilizing the steady state and stabilizing a limit cycle (periodic state). The frequency of the emerging oscillations depends on neuronal and non-neuronal parameters characterizing the oscillatory circuit. The constant input c_1 (see Eq. (1) in Materials and Methods) coming to the head interneurons from other head neurons or/and sensory input can abolish oscillations if it is either too inhibitory or too excitatory. Thus, depending on the activity level of the head neural networks, a worm can decide when to start or to stop moving. Our theoretical analysis (below) shows that models A and B give very similar results for all model parameters, except for the coupling strength and time constant of the stretch receptors.

Oscillations generated in the head are imposed on the body wall nervous system primarily through interconnections of the body wall muscles with the head muscles, and then via body wall stretch receptors and synapses. However, the electric coupling between muscles and synaptic coupling between neurons cannot be too weak, since then oscillations along the body wall are unsustainable and their amplitude (waveform) decays with a distance from the head (Fig. 7A,B, lower panels). In our model the stability for the oscillations is provided by the interneurons AVB and PVC. Since these neurons receive a massive oscillatory input with different phases in the head (from X, Y, Z), their resulting activities are only weakly- or non-oscillatory, because of a partial

or complete cancellation of the input oscillatory phases. Nearly constant input from AVB and PVC to excitatory motor neurons overcomes their inhibition from the DVA neuron and stabilizes undulatory oscillations, with ventral and dorsal sides in anti-phase (see also Discussion). This input in combination with sufficiently strong synapses and gap-junctions ensure that the oscillatory waveform does not decay with a distance from the head. Consequently, the distribution of frequencies along the body is homogeneous despite the fact that rhythm is generated in the head. This homogeneity is consistent with the experimental results for wild-type and all non-neuronal mutants (Figs. 3, 4 and 7; Suppl. Table T1). For the distribution of frequency of neuronal mutants with weak synapses see the Discussion.

Wave generation and wavelength constancy. Undulatory movement also requires a neuromuscular wave (Karbowski et al, 2006). Our model for forward locomotion can generate such a wave due to a non-local stretch receptor activity transduced to the body wall somas of excitatory motor neurons via their long unidirectional dendrites (Fig. 2). With a posterior stretch receptor coupling the wave propagates posteriorly (corresponding to forward motion), while with an anterior stretch receptor coupling the wave propagates anteriorly (corresponding to backward motion) (Fig. 8A,B). Thus, the directionality of the wave (and thus motion direction) depends only on the directionality of the long dendrites. Unidirectional stretch receptor feedback along the body wall is critical for locomotion, since when it is absent the wave does not propagate. In this case oscillations are also abolished in model B, although in model A they are still present (due to an intrinsically oscillatory interneuron loop $X \rightarrow Y \rightarrow Z \rightarrow X$). The correlation between

directions of the wave and a hypothetical stretch receptor coupling is consistent with the neuroanatomical details of the corresponding body wall excitatory motor neurons of type A and B, controlling backward and forward motion, respectively. These neurons have long undifferentiated dendrites directed in opposite directions (White et al, 1986). The phase differences between neighboring muscle activities along the body wall are to a large extent stable over time and essentially frequency independent (Fig. 8C). Since, in general, a phase lag is inversely proportional to wavelength, this implies that the wavelength is also frequency independent. The intermuscle phase lag depends, however, on the stretch receptor coupling, although very weakly if coupling is sufficiently strong (Fig. 8D).

Biphasic dependence of frequency on synaptic coupling. Chemical coupling via synapses is one of the critical parameters in the circuit, since it can potentially affect numerous kinematic characteristics. Our model makes predictions about the influence of inhibitory and excitatory transmission on frequency. In Fig. 9A,B, we plot the dependence of the frequency on the inhibitory synaptic strength at the neuromuscular junction. This dependence exhibits a non-monotonic (biphasic) relationship. For weak inhibitory strength, the frequency is small and it increases with increasing inhibition up to some maximal value, and then it decreases.

With respect to excitation, our model shows that frequency is a biphasic function of the global excitatory synaptic strength (Fig. 9C,D), similar to the above case of inhibition. When the excitation level is either above or below some critical values, the oscillations become unstable and movement disappears. For the consistency of these

results with the experimental data see the section "Comparison of the theory with the experimental data".

The origin of the biphasic relationships between the frequency and inhibitory and excitatory synaptic strengths lies in the shapes of temporal muscle voltage characteristics (Fig. 9E,F). For weak inhibition (or strong excitation) muscle voltage increases sharply but its relaxation phase is prolonged as compared to the case of intermediate levels of inhibition (or excitation). In contrast, for strong inhibition (or weak excitation) the muscle voltage increases slowly but its decay phase is much faster. In both regimes, corresponding longer decay or rise phases of the muscle voltage cause the frequency drop in comparison to the intermediate regime (Fig. 9E,F).

Frequency vs. gap-junction coupling. Electrical coupling via gap junctions plays also a significant role in coordination of the circuit components. Models A and B both predict that frequency is a monotonically increasing function of the muscle gap junction conductance strength (Fig. 10A,B). Moreover, when this gap junction coupling is too weak, the oscillatory signal coming from the head fails to propagate down the body, i.e., the neuromuscular wave is attenuated, causing defective locomotion. On the other hand, when this coupling is too strong the wave disappears because the whole system is synchronized. Thus, for a robust wave the gap-junction coupling should be in an intermediate range.

Frequency vs. muscle calcium signaling. In our model, the amount of calcium influx in muscles is controlled by the coupling w_{mm} (Eqs. 6 and 12). In Fig. 10C,D, we display

the biphasic or triphasic dependence of frequency on this amplitude. At some very high level of calcium signaling oscillations become unstable and the system converges to a steady-state, in which undulatory motion is abolished. The curves in Fig. 10C,D are qualitatively distinct from the biphasic curves for global excitation and inhibition presented in Fig. 9, since the latter exhibit pronounced local maxima.

Frequency vs. stretch receptor coupling. One of the roles of the stretch receptor feedback coupling is to modulate the undulatory rhythm. We find that models A and B differ only for a weak stretch receptor coupling. However, if the coupling is sufficiently strong, both models show that frequency increases slightly with increasing the coupling (Fig. 11).

Frequency vs. time constants. We also tested how the frequency of oscillations depends on various time constants associated with different dynamic variables. In general, an increase in any of the time constants causes decrease in frequency, with a variable sensitivity among different time constants. As an example, in Fig. 12 we show the dependence of frequency on the muscle membrane time constant τ_m (Fig. 12A), and on the stretch receptor time constant τ_s (Fig. 12B). Models A and B differ only for small values of time constants.

Comparison of the theory with the experimental data

Below we make a qualitative comparison of several of our theoretical results to either

our data or to the data already published.

- *Invariance of neuromuscular wavelength.* This experimental result (Table 2; see Karbowski et al. (2006) for a larger data set) is consistent with our theory, which shows that intermuscle phase lag is practically frequency independent (Fig. 8C), and is only weakly stretch receptor coupling dependent if this coupling is sufficiently strong (Fig. 8D). The latter result can explain wavelength constancy across different nematode species (Karbowski et al, 2006).

- *Biphasic dependence of frequency on synaptic coupling.* For inhibitory coupling this experimental result (Fig. 5) is consistent with our theory (Fig. 9A,B). Moreover, the theoretical curve suggests that wild-type worms may have GABA coupling parameters close to the optimal values.

  In the case of excitatory coupling, data in Fig. 6A for acetylcholine signaling are not in conflict with the theoretical biphasic relationship (Fig. 9C,D), although they are not conclusive. However, the support for the biphasic relation between frequency and acetylcholine signaling comes from combining the experimental results in Fig. 6B, containing *slo-1* worms with transgenes, with our previously published data (Karbowski et al, 2006) on hyperactive *goa-1(n1134)*, *goa-1(sy192)*, and *egl-30(tg26)* mutants (Segalat et al, 1995; Mendel et al, 1995). Both

of these groups have increased acetylcholine synaptic signaling above wild-type level but their corresponding undulatory frequencies show the opposite behavior. In the case of *slo-1* worms with transgenes, the frequency slightly decreases as compared to animals with the wild-type levels of neurotransmission (Fig. 6B), while in the case of hyperactive mutants the frequency increases (Karbowski et al, 2006). This behavior clearly suggests a non-monotonic, possibly biphasic dependence, in agreement with our theoretical results (Fig. 9C,D).

- *Frequency increases (decreases) monotonically with increasing (decreasing) muscle gap-junction coupling.* This theoretical result (Fig. 10A,B) agrees with the recent experimental results on *unc-9(fc16)* mutants (Liu et al, 2006). These mutants have body wall muscle gap junction conductance severely reduced (but neurotransmission at neuromuscular junction unaffected) and velocity much lower than wild type (Liu et al, 2006). As velocity and frequency are linearly related (see Karbowski et al, 2006), this implies that in *unc-9(fc16)* worms the frequency is also strongly reduced, as our theory predicts (Fig. 10A,B).

- *Frequency decreases monotonically with increasing model time constants.* This theoretical result (Fig. 12) is consistent with the data on *unc-54* mutants. These mutants have significantly increased time constant characterizing the duration of the cross-bridge cycle formation between myosin and actin (Moerman and Fire, 1997) and their undulatory fre-

quency is much smaller than wild type (Fig. 3A,B; Suppl. Table T1). In our model, Eqs. (1-13), this slowing down of the contraction-relaxation cycle corresponds to an increase of the muscle membrane time constant τ_m.

Discussion

In this paper, we use a combined approach involving genetic perturbations, quantitative behavioral tracking, and mathematical modeling to uncover the mechanisms of *C. elegans* locomotion. Our circuit model is detailed enough to be biologically realistic and yet not excessively complex to obscure the basic mechanisms. We hope this model provides a link between molecular/cellular and systems level of understanding.

Discussion of the main results

We propose the existence of a mechanosensory feedback in *C. elegans* that strongly affects locomotion. Feedback coupling is implied by our locomotory data on non-neuronal mutants (Fig. 4; Suppl. Table T1), in which neural function is not affected directly and yet they exhibit abnormal locomotion as compared to wild type. In particular, these non-neuronal mutants have significantly modified frequency and flex of undulations, which are indirectly linked to the activation levels of the motor neurons. The conclusion about the existence of the mechanosensory feedback is also compatible with previous experimental data suggesting that altered mechano-sensory channels can profoundly affect locomotory pattern. For example, *C. elegans unc-8* mutants, which have defective putative mechanosensory channels, display abnormal locomotion (Tavernarakis et al, 1997). Also recent results on the mechanosensory TRPN channel TRP-4 show that it is involved in nematode bending control (Li et al, 2006). Experimental data indicate that some neurons serve as mechanosensors with specialized sensing channels, mostly in the head and tail (Goodman and Schwarz, 2003; Suzuki et al, 2003; Wicks

et al, 1996). In the theoretical model of the locomotory circuit, we implemented the mechanosensory feedback as a stretch receptor coupling in the head and in the body wall. Its role, however, is different in both of these circuits. In the head, the stretch feedback participates in the control or generation of oscillations, while in the body wall, in addition, it generates the neuromuscular wave by breaking a spatial longitudinal symmetry of the system through unidirectional coupling between body wall components. Possible neural candidates for the stretch receptors are: a pair of SAA neurons in the head, and VB and DB motor neurons along the body wall, because of their long undifferentiated processes (White et al, 1986).

The remarkable experimental finding (Fig. 3 and Suppl. Table T1) is that the opposite motions - forward and backward - exhibit spatial gradients of flex and in the case of neuronal mutants also weak frequency gradients directed in the same way, i.e., from the head to the tail. This finding might suggest that primary oscillations are generated in the same location for both types of motion. Where could this location be? Because in most cases signals propagating through a biological tissue get attenuated as a result of energy dissipation caused by tissue viscosity, the most likely candidate for a primary pacemaker (CPG) in *C. elegans* is the head. Below, we argue that other potential candidates for the primary CPG, i.e. either tail or body wall or some combination, are less likely.

If tail served as a primary oscillator, then according to Fig. 3, this would require amplification of the signal as it travels from the tail to the head, which in turn, would require large amounts of mechanical energy generated in the body wall to compensate

for energy loss. Small number and low linear density of the body wall motor neurons (37 forward motion motor neurons (VB, DB, VD, DD) cover ~ 80 % of the body length as compared to ~ 200 neurons in the head; see White et al, 1986), and the decaying trend of synaptic density toward the tail (Fig. 7B in Chen et al, 2006) are probably not sufficient to excessively activate body wall muscles and achieve signal amplification. Another possibility is that both head and tail are two separate primary pacemakers with two distinct spontaneous frequencies. However, because head and tail have numerous recurrent synaptic connections, these two potential oscillators would likely adjust their frequencies to a single one, as happens in a system of coupled oscillators (e.g. see Strogatz, 1994). Some neuronal mutants show that head and tail oscillate differently, which is a strong evidence against such a scenario. It is important to stress that our hypothesis about the primary oscillator in the head does not exclude the tail from being a secondary oscillator. This potential oscillator could be activated only by an outside source, either by head neurons or by a mechanical stimulation (e.g. tail tapping). In fact, since the tail has the second largest density of neurons in *C. elegans* (Chen et al, 2006), it is potentially capable of a slight signal amplification, as is evident from flex data for some mutants near their tails (signal amplification is possible because a typical muscle cell in the tail should get more excitation than a typical muscle cell in the body wall due to a higher neural density in the tail). Finally, there also exists a theoretical possibility that the body wall motor neurons serve as a primary CPG. This hypothesis is, however, not compatible with our experimental results on posterior gradients of body undulations, i.e., one would expect more uniform spatial distributions. Other

arguments against this possibility are: the non-zero flex of GABA null mutants (Table T1 in the Suppl. Information) and older data on interneuron ablation (Chalfie et al, 1985). GABA null mutants have functionally disabled ventral-dorsal cross-inhibition at the neuromuscular junction along the body wall (such cross-inhibition is necessary for body undulations). Despite this deficiency, they have non-zero flexes, which is a clear indication that anti-phase undulations must be imposed from another part of the body. By the same token, ablation of the two forward motion interneurons AVB and PVC have been shown to virtually abolish (or strongly reduce) body wall undulations and the forward motion but still keep intact the head undulations (Chalfie et al, 1985). This experiment suggests that forward motion body wall oscillations are not sustainable without the presence of connections to the head (which again is in support of our hypothesis that the head serves as a primary CPG). We want to stress, however, that the body wall motor neurons might serve as a secondary short-term pacemaker when stimulated from outside, similar to the tail.

The most interesting consequences of our theoretical model are the biphasic nature of the dependence of frequency on the global strength of synaptic coupling (Fig. 9) and on muscle calcium signaling (Fig. 10C,D), as well as the constancy of neuromuscular wavelength (Fig. 8C,D). The biphasic relationships, being a direct consequence of the non-linearities present in the system, are in agreement with the experimental data on GABA signaling (Fig. 5), and acetylcholine signaling (Fig. 6) if combined with a previously published kinematic results on hyperactive acetylcholine mutants (Karbowski et al. 2006). These results may suggest that wild-type worms have synaptic couplings

close to their optimal values. The stability of the neuromuscular wave is determined by the ability of the locomotory circuit to maintain the precise phase relationships between body components. Our model shows that unidirectional stretch receptor coupling involving long dendrites of the body wall motor neurons (Fig. 2) provides a mechanism for such a coherency, since the phase differences between neighboring muscles and consequently the wavelength are stable and practically frequency and stretch receptor coupling independent (Fig. 8C). The invariance of the wavelength agrees well with the experimental data in Table 2 and in Karbowski et al (2006).

Within our theoretical model, we consider two extreme forms of CPG in the head circuit. In model A, the primary oscillations are generated on the level of head interneurons and then only modulated by stretch receptor feedback, and ultimately by the whole locomotory network, which makes oscillations more robust. In model B, oscillations in the head emerge as a result of collective loop interactions between head neurons, muscles and stretch receptors, without prior oscillatory activity of neurons. In this scenario, the stretch receptor feedback is a critial element in creating oscillations, unlike in model A. These two mechanisms can be realized in the same circuit with the same topology, only with different parameters characterizing head interneurons interactions, and worms can potentially use either of these mechanisms by modulating their respective parameters (change in only few of them is needed to transit between models A and B). The presence of oscillations can be controlled by sensory input that can change the level of excitation coming to head interneurons, which is controlled in our model by the parameter c_1. In general, both excessive excitation (large positive

c_1) and excessive inhibition (large negative c_1) abolish the oscillations and consequently the motion. From a mathematical perspective, oscillations in the circuit are the result of non-linear feedback loops, which cause temporal delays in the system and make the steady state unstable. This mechanism is quite general and robust (insensitive on the precise values of parameters) and appears in many biological and non-biological (e.g. engineering) systems (Strogatz, 1994). It is important to stress that both of the above potential forms of CPG are indistinguishable on a phenotypic level, if stretch receptor coupling is sufficiently strong and slow (Figs. 9-12). In this regime, both models yield qualitatively similar predictions regarding dynamic properties of the locomotory circuit under different perturbations, and both are consistent with the experimental data. This fact suggests that global locomotory output is to a large extent a result of the collective dynamics of the whole circuit, not just its local elements, and it does not depend on a specific mechanism of oscillation generation in most of the parameter space. In our model, the head interneuron circuitry is treated in a simplified manner given the complexity of the actual circuitry. This simplified approach, however, captures an important feature of interneuron connectivity pattern, namely small-scale feedback loops. The model head interneurons X, Y, Z form a minimal circuit (loop) in *C. elegans* that can generate robust oscillations. In general, our results suggest that more experimental attention should be paid to the head circuit in the context of locomotion.

Discussion of additional aspects of this study

Our theoretical study shows the existence of several "windows of parameters" (usually sufficiently wide) for the presence of undamped oscillations along worm's body,

which is required for a sustained undulatory motion. Beyond those critical ranges of parameters oscillations decay just after a few cycles, with the most pronounced decay for posterior parts of the circuit. For example, the global levels of excitation and inhibition in the network can be neither too small nor too large for the stable oscillations (Fig. 7). The weak frequency gradients we observe experimentally for neuronal mutants with compromised synaptic transmission (Figs. 3, 5 and 6; Suppl. Tables T1, T2) may be directly related to the spatial decay of the waveform along the body, which we notice in simulations (Fig. 7A,B lower panels). In particular, our simulations indicate that for mutants with weak synaptic coupling the more posterior a given muscle is the more damped are its oscillations. It seems that our automated experimental setup has problems with detecting low amplitude oscillations (low signal-to-noise ratio) in more posterior parts, which manifests itself in weak frequency gradients.

Similarly, muscle calcium signaling cannot be too large to maintain undulatory locomotion. Experiments by Maryon et al. (1996, 1998), in which wild-type worms were exposed to ryanodine, are consistent with the last prediction. Worms treated with ryanodine, which produces an excessive amount of calcium in muscle cells, are either very sluggish or completely paralyzed (Maryon et al, 1996).

In our model, the activity of AVB and PVC has two other important functions. First, to make oscillations in the body wall circuit (imposed from the head via muscles and stretch receptors) more robust by releasing excitatory motor neurons (VB and DB) from inhibitory influence of DVA (when this inhibition is too strong or a signal from AVB and PVC too weak oscillations are not sustained). Second, to start the

posterior neuromuscular wave by signaling to VB and DB motor neurons with the help of their long posterior dendrites. This wave is a second critical factor for the forward locomotion, as is evident from a biomechanical model of worm's undulations (Karbowski et al, 2006). Following the Byerly and Russell hypothesis we assume that long dendrites contain stretch receptors that provide posterior coupling between spatially separated parts of the body wall. Without this coupling, the wave is abolished in both models A and B. The involvment of stretch receptors in generation of the wave was also suggested before on purely biomechanical grounds (Niebur and Erdos, 1993). It is important to stress that forward and backward motion require neuromuscular waves traveling in opposite directions, which are correlated with the corresponding opposite directions of the motor neuron's dendrites in forward and backward circuits. However, based on the above arguments it seems that both types of motion have CPG's located probably in the head.

In the model, spontaneous collective oscillations can be also generated in the body wall circuit without the involvement of the head circuit and/or AVB and PVC interneurons, because of the numerous feedback loops present in the body wall. This mechanism was theoretically considered by Bryden and Cohen (2004). We did not, however, pursue this possibility for the reasons outlined above. Therefore, the parameters in our model are chosen such that the body wall neural circuit does not oscillate in isolation from the head circuit, i.e., when AVB and PVC neurons are removed and when there is no coupling between muscles in the head and the body wall. In particular, we assumed that the excitatory (VB, DB neurons) and inhibitory (VD, DD neurons) motor neurons

are intrinsically non-oscillatory.

Our theoretical results show, for both models A and B, that frequency increases weakly with increasing the stretch receptor coupling if it is strong enough (Fig. 11). This theoretical result is consistent with data for *trp-4* mutants (Li et al, 2006) and cuticle *sqt-1* mutants. These animals show the opposite behavior, i.e., *trp-4* are faster and have larger flex than wild-type (Li et al, 2006), while *sqt-1* are slower and have smaller flex (Suppl. Table T1). Decreased (increased) flex angle implies smaller (larger) stretching, which in turn suggests weaker (stronger) stretch receptor feedback coupling, and according to our theory, lower (higher) frequency. The case of BE109 mutants is more complex, since they exhibit higher flex angle and lower frequencies than the wild-type worms (Suppl. Table T1). The likely explanation in this case is that despite higher flexes the actual stretch receptor coupling might be smaller than in wild-type. This is possible because these mutants are noticeably shorter than wild type (about 20%), suggesting a profound structural changes in the cutico-skeletal system that might affect the quality of a mechano-sensory signaling.

C. elegans locomotion seems similar to the locomotion of other systems performing undulations. However, there are also some important differences, in particular, other undulatory systems such as leech, lamprey, and crayfish have anatomically well defined body segments, which serve as local CPG's (Skinner and Mulloney, 1998; Friesen and Cang, 2001; Marder et al, 2005). In contrast, *C. elegans* lacks body segments (White el al, 1986) and its body wall seems to be rather passive in comparison to the head, which likely serves as CPG.

We note that our circuit model allows a direct investigation of the effects of single- or multi-neuron ablations (e.g. motor neurons) on locomotion characteristics. By comparing kinematic parameters of *C. elegans* with ablations to circuit model predictions one can in principle gain information on the strength of some synaptic connections and refine the model.

Some of our extrachromosomal transgene constructs involving *slo-1* mutants might not precisely restore the wild-type functions. However, because our analysis of the experimental data is to a large extent qualitative, the possible under- or over-shooting to the wild-type level are not critical to our conclusions.

Conclusions

Our major conclusions are: (i) based on the anterior-to-posterior gradients of the flex for almost all strains, and partly based on the corresponding weak gradients of the frequency for neuronal mutants, the most likely location of CPG for both forward and backward locomotion is the head, (ii) stretch receptor feedback associated with long unidirectional dendrites in the body wall plays a critical role in neuromuscular wave generation and conservation of the wavelength, (iii) there exist optimal values of synaptic couplings (both inhibitory and excitatory) for which frequency of undulations is maximal, and wild-type worms might be close to that optimal regime, (iv) the precise mechanism of oscillation generation within CPG, i.e., whether neural activity or reflex activity dominate, is irrelevant and indistinguishable on a phenotypic level, except for weak and fast stretch receptor coupling, (v) frequency increases monotonically with muscle gap-junction strength, and (vi) frequency decreases monotonically with increas-

ing time constants of the circuit elements. Our circuit model can also make predictions: (i) frequency should depend in a non-monotonic manner on muscle calcium signaling, and (ii) long dendrites of the excitatory motor neurons in the body wall are critical for generating neuromuscular wave and thus perturbing them should perturb the wavelength. Experiments addressing these problems would either provide additional support for our model or cast doubt on some assumptions, thus helping in refining the model.

Acknowledgments

We thank A. Davies and S. McIntire for *slo-1* strains, and J. Kramer for advice on cuticle mutants. The work was supported by the Sloan-Swartz Fellowship (J.K.), by NIH Fellowship (NS043037 to G.S.), by USPHS grant R01-DA018341 (P.W.S.), and by the Howard Hughes Medical Institute, with which P.W.S. is an Investigator.

References

Akay T, Haehn S, Schmitz J, Buschges A (2004). Signals from load sensors underline interjoint coordination during stepping movements of the stick insect leg. *J. Neurophysiol.* 92: 42-51.

Bargmann CI (1998). Neurobiology of the *Caenorhabditis elegans* genome. *Science* 282: 2028-2033.

Brenner S (1974). The genetics of *Caenorhabditis elegans*. *Genetics* 77: 71-94.

Bryden J, Cohen N (2004). A simulation model of the locomotion controlers for the

nematode *Caenorhabditis* elegans. In: Schaal S et al editors. From Animals to Animats 8: Proc. Eight Intern. Conf. on Simulation of Adaptive Behavior. Cambridge: MIT Press, pp 183-192.

Chalfie M, White J (1988). *The Nervous System.* In: Wood WB, editor. The Nematode *Caenorhabditis elegans.* Cold Spring Harbor: Cold Spring Harbor Laboratory Press, pp. 337-391.

Chalfie M et al (1985). The neural circuit for touch sensitivity in *Caenorhabditis elegans. J. Neurosci.* 5: 956-964.

Chen BL, Hall DH, Chklovskii DB (2006). Wiring optimization can relate neuronal structure and function. *Proc. Natl. Acad. Sci. USA* 103: 4723-4728.

Cronin CJ et al. (2005). An automated system for measuring parameters of nematode sinusoidal movement. *BMC Genet.* 6: 5.

Davis RE, Stretton AOW (1989). Signaling properties of *Ascaris* motorneurons: graded active responses, graded synaptic transmission and tonic transmitter release. *J. Neurosci.* 9: 415-425.

Davies AG et al (2003). A central role of the BK potassium channel in behavioral responses to ethanol in *C. elegans. Cell* 115: 655-666.

Delcomyn F (1980). Neural basis of rhythmic behavior in animals. *Science* 210: 492-498.

de Bono M, Maricq AV (2005). Neuronal substrates of complex behaviors in *C. elegans. Annu. Rev. Neurosci.* 28: 451-501.

Francis MM, Mellem JE, Maricq AV (2003). Bridging the gap between genes and

behavior: recent advances in the electrophysiological analysis of neural function in *Caenorhabditis elegans*. *Trends Neurosci.* 26: 90-99.

Friesen WO, Cang J (2001). Sensory and central mechanisms control intersegmental coordination. *Curr. Opin. Neurobio.* 11: 678-683.

Gengyo-Ando K et al. (1993). The *C. elegans unc-18* gene encodes a protein expressed in motor neurons. *Neuron* 11: 703-711 (1993).

Goodman MB, Hall DH, Avery L, Lockery SR (1998). Active currents regulate sensitivity and dynamic range in *C. elegans* neurons. *Neuron* 20: 763-772.

Goodman MB, Schwarz EM (2003). Transducing touch in *Caenorhabditis elegans*. *Annu. Rev. Physiol.* 65: 429-452.

Gray JM, Hill JJ, Bargmann CI (2005). A circuit for navigation in *Caenorhabditis* elegans. *Proc. Natl. Acad. Sci. USA* 102: 3184-3191.

Grillner S (1975). Locomotion in vertebrates: central mechanisms and reflex interaction. *Physiol. Rev.* 55: 247-303.

Hobert O (2003). Behavioral plasticity in *C. elegans*: Paradigms, circuits, genes. *J. Neurobiol.* 54: 203-223.

Jin Y et al (1999). The *Caenorhabditis elegans* gene *unc-25* encodes glutamic acid decarboxylase and is required for synaptic transmission but not synaptic development. *J. Neurosci.* 19: 539-548.

Jospin M, Jacquemond V, Mariol MC, Segalat L, Allard B (2002). The L-type voltage-dependent Ca^{2+} channel EGL-19 controls body wall muscle function in *Caenorhabditis elegans*. *J. Cell Biol.* 159: 337-347.

Karbowski J, Cronin CJ, Seah A, Mendel JE, Cleary D, Sternberg PW (2006). Conservation rules, their breakdown, and optimality in *Caenorhabditis* sinusoidal locomotion. *J. Theor. Biol.* 242: 652-669.

Lee RYN, Lobel L, Hengartner M, Horvitz HR, and Avery L (1997). Mutations in the $\alpha 1$ subunit of an L-type voltage-activated Ca^{2+} channel cause myotonia in *Caenorhabditis elegans*. *EMBO J.* 16: 6066-6076.

Li W, Feng Z, Sternberg PW, Xu XZS (2006). A *C. elegans* stretch receptor neuron revealed by a mechanosensitive TRP channel homologue. *Nature* 440: 684-687.

Liu Q, Chen B, Gaier E, Joshi J, Wang Z-W (2006). Low conductance gap junctions mediate specific electrical coupling in body-wall muscle cells of *Caenorhabdidtis elegans. J. Biol. Chem.* 281: 7881-7889.

Maduro M, Pilgrim D (1995). Identification and cloning of unc-119, a gene expressed in the *Caenorhabditis elegans* nervous system. *Genetics* 141: 977-988.

Marder E, Calabrese RL (1996). Principles of rhythmic motor pattern generation. *Physiol. Rev.* 76: 687-717.

Marder E, Bucher D, Schulz DJ, Taylor AL (2005). Invertebrate central pattern generation moves along. *Curr Biology* 15: R685-R699.

Maryon EB, Coronado R, Anderson P (1996). *unc-68* encodes a ryanodine receptor involved in regulating *C. elegans* body-wall muscle contraction. *J. Cell Biol.* 134: 885-893.

Maryon EB, Saari B, Anderson P (1998). Muscle-specific functions of ryanodine receptor channels in *Caenorhabditis elegans*. *J. Cell Sci.* 111: 2885-2895.

McIntire SL, Jorgensen E, Kaplan J, Horvitz HR (1993). The GABAergic nervous system of *Caenorhabditis elegans*. *Nature* 364: 337-341.

Mendel JE et al (1995). Participation of the protein Go in multiple aspects of behavior in C. elegans. Science 267: 1652-1655.

Moerman DG, Fire A (1997). *Muscle: Structure, Function, and Development.* In: Riddle DL et al. editors. C. elegans II. Cold Spring Harbor: Cold Cold Spring Harbor Laboratory Press, pp. 417-470.

Niebur E, Erdos P (1991). Theory of the locomotion of nematodes. *Biophys. J.* 60: 1132-1146.

Nusbaum MP, Beenhakker MP (2002). A small-systems approach to motor pattern generation. *Nature* 417: 343-350.

Okuda T, Haga T, Kanai Y, Endou H, Ishihara T, Katsura I. (2000). Identification and characterization of the high-affinity choline transporter. *Nature Neurosci.* 3: 120-125.

Schuske K, Beg AA, Jorgensen EM (2004). The GABA nervous system in *C. elegans*. *Trends Neurosci.* 27: 407-414.

Segalat L, Elkes DA, Kaplan JM (1995). Modulation of serotonin-controlled behaviors by Go in Caenorhabditis elegans. *Science* 267: 1648-1651.

Skinner FK, Mulloney B (1998). Intersegmental coordination in invertebrates and vertebrates. *Curr. Opin. Neurobiol.* 8: 725-732.

Strogatz SH (1994). *Nonlinear Dynamics and Chaos*. Westview Press.

Suzuki H et al (2003). In vivo imaging of *C. elegans* mechanosensory neurons demonstrates a specific role for the MEC-4 channel in the process of gentle touch sensation.

Neuron 39: 1005-1017.

Tavernarakis N, Shreffler W, Wang S, Driscoll M (1997). unc-8, a DEG/ENaC family member, encodes a subunit of a candidate mechanically gated channel that modulates *C. elegans* locomotion. *Neuron* 18: 107-119.

Wang ZW, Saifee O, Nonet ML, Salkoff L (2001). Slo-1 potassium channels control quantal content of neurotransmitter release at the *C. elegans* neuromuscular junction. *Neuron* 32: 867-881.

Weimer R.M., et al. (2003). Defects in synaptic vesicle docking in *unc-18* mutants. *Nature Neurosci.* 6: 1023-1030.

White JG, Southgate E, Thomson JN, Brenner S (1986). The structure of the nervous system of the nematode *Caenorhabditis elegans. Phil. Trans. R. Soc. Lond.* B 314: 1-340.

Wicks SR, Roehrig CJ, Rankin CH (1996). A dynamic network simulation of the nematode tap withdrawal circuits: Predictions concerning synaptic function using behavioral criteria. *J. Neurosci.* 16: 4017-4031.

Table 1: Parameters used in simulations of Eqs. (1)-(13).

Parameter		Parameter		Parameter	
τ_x	130 ms	τ_y	100 ms	τ_z	150 ms
τ_e	150 ms	τ_i	120 ms	τ_m	200 ms
τ_s	350 ms	τ_{avb}	165 ms	τ_{pvc}	150 ms
c_1	1.0	c_2	-1.0		
$\tilde{w}_{me}$	q_{ex}	$\tilde{w}_{mi}$	$0.5q_{in}$	w_{xz}	0.6
w_{zx}	q_{ex}	w_{ey}	$0.5q_{ex}$	w_{xi}	$0.3\tilde{w}_{mi}$
w_{yx}	$0.5q_{ex}$	w_{zy}	$0.5q_{ex}$	w_{es}	0.4
w_{xs}	$5.0w_{es}$	w_{ie}	$1.5q_{ex}$	w_{me}	$0.5q_{ex}$
w_{mi}	$0.3q_{in}$	w_{sm}	0.5	w_{mm}	0.1
$w_{e,pvc}$	$0.2q_{ex}$	$w_{avb,pvc}$	$0.2q_{ex}$	$w_{avb,x}$	$0.4q_{ex}$
$w_{pvc,x}$	$0.2q_{ex}$				
g_{avb}	0.10	g_m	0.10	g_e	0.05
g_i	0.05	$g_{avb,e}$	0.10		
θ_{me}	0.55	θ_{mi}	0.40	θ_{xz}	0.25
θ_{zx}	0.35	θ_{ey}	0.30	θ_{xi}	0.40
θ_{yx}	0.30	θ_{zy}	0.35	θ_{es}	0.20
θ_{xs}	0.20	θ_{ie}	0.55	θ_{sm}	0.00
θ_{mm}	0.55	$\theta_{e,pvc}$	0.45	$\theta_{avb,pvc}$	0.45
$\theta_{avb,x}$	0.18	$\theta_{pvc,x}$	0.20		
η_{me}	0.80	η_{mi}	1.20	η_{xz}	0.02(A),0.20(B)
η_{zx}	0.05(A),0.65(B)	η_{ey}	0.05(A),0.80(B)	η_{xi}	1.20
η_{yx}	0.05(A),0.80(B)	η_{zy}	0.05(A),0.65(B)	η_{es}	0.03
η_{xs}	0.03	η_{ie}	0.80	η_{sm}	0.05
η_{mm}	2.40	$\eta_{e,pvc}$	1.00	$\eta_{avb,pvc}$	1.00
$\eta_{avb,x}$	0.60	$\eta_{pvc,x}$	0.60		

Inhibitory w_{xz} is assumed to be non-GABA-ergic. Labels (A) and (B) refer to models A and B.

Table 2: Body length normalized wavelength during forward and backward locomotion for adult wild-type (WT) *C. elegans* and mutants.

Genotype	Normalized wavelength	
	Forward motion	Backward motion
C. elegans WT (N=62)	0.61±0.3	0.64±0.07
Neuronal Mutants:		
unc-25(e156) (N=4)	0.68±0.01	0.69±0.04
unc-46(e177) (N=4)	0.71±0.01	0.71±0.02
unc-18(e81); cho-1::unc-18::yfp (N=14)	0.70±0.03	0.71±0.07
slo-1(js118) (N=18)	0.62±0.02	0.64±0.02
Non-neuronal Mutants:		
egl-19(n582); unc-119::egl-19::yfp		
Line A (N=16)	0.64±0.03	0.67±0.13
Line B (N=16)	0.63±0.03	0.66±0.07
unc-68(r1158) (N=16)	0.62±0.03	0.62±0.06

Figure Legends

Fig. 1

The general approach taken in this paper. (A) We perturb (manipulate) genes whose products affect some properties of different classes of neurons and other non-neuronal parameters. These altered properties, in turn, affect locomotory characteristics. The locomotory pattern may affect activities of neurons via mechanosensory feedback. (B) Actual image of a worm with superimposed reference points measuring worm's coordinates. Based on a spatio-temporal pattern of each of these points we calculated motion characteristics. The maximal angle over time between two solid lines (green and red on-line) determines the half of a local flex angle, which quantifies a deviation from a straight line of two neighboring reference body sections during motion. Dashed arrow (blue on-line) indicates the direction of motion). Adapted from Cronin et al. (2005).

Fig. 2

Schematic diagram of the circuit for forward locomotion in the nematode *C. elegans*. Excitatory synapses are denoted by arrows ($\rightarrow$), inhibitory synapses by bars ($\dashv$), and electric gap junctions by dashed lines ($--$). (A) The large scale view of the circuit. Head neurons excite and inhibit head muscles (ventral M_{hv} and dorsal M_{hd}), and additionally receive feedback from head stretch receptors (ventral S_{hv} and dorsal S_{hd}). The signal from the head neurons is transmitted to the body wall circuit through two interneurons AVB and PVC (with very long dendrites spanning the whole body length), and through the gap junction coupling between head and body wall (M_v and M_d) muscles. Body wall excitatory motor neurons (ventral VB and dorsal DB) use acetylcholine

for synaptic signaling. These neurons have elongated processes directed posteriorly, which, we assume, contain stretch receptors (S). Stretch receptors detect relative differences in the activities of the corresponding ventral and dorsal muscles. Body wall inhibitory motor neurons (ventral VD and dorsal DD) use GABA for synaptic signaling. These neurons act as cross-inhibitors, since their only input is from the opposite side excitatory motor neurons. Excitatory motor neurons as well as inhibitory motor neurons are connected within each group by gap junctions (not shown). Also, excitatory motor neurons (VB and DB) receive synaptic input from DVA interneuron, which we assume is inhibitory. (B) Schematic diagram of the head CPG. The head interneurons X (corresponding to SAA neuron) and Y are excitatory and, we assume, signal with acetylcholine, while Z is inhibitory and, we assume, signals without GABA (GABA is expressed only in one head interneuron RIS and its ablation does not influence phenotype; see Schuske et al, 2004). Ventral and dorsal groups of these interneurons effectively inhibit each other such that oscillatory rhythm in the head alternates between ventral and dorsal sides. Head excitatory motor neurons (E_{hv} and E_{hd} corresponding, e.g., to pairs of SMB and SMD neurons) use acetylcholine, and head inhibitory motor neurons (I_{hv} and I_{hd} corresponding to a pair of RME neurons) use GABA for synaptic signaling. As in the body wall, stretch receptors in the head (S_{hv} and S_{hd}) detect relative differences in the ventral and dorsal activities of head muscles (M_{hv} and M_{hd}). The primary oscillations can be generated either within the X, Y, Z loop or with a stretch receptor feedback within the X, Y, E, M, S loop. Changes in the level of global excitation (acetylcholine) and inhibition (GABA) affect frequency of these oscillations.

Fig. 3

Experimental examples of distributions of the undulatory frequency and bending flex angle along the worm's body for forward and backward motion. (A), (B) Frequency is relatively uniform during forward and backward motion for wild type (solid blue line) and non-neuronal mutants *unc-68(r1158)* (dashed-dotted green line) and *unc-54(s74)* (dotted black line), but it decays weakly towards the tail for GABA defective *unc-25(e156)* mutant in forward locomotion (dashed red line). (C), (D) Flex angle decays markedly posteriorly for all these animals, in some cases, with an increase towards the tail (notably for *unc-54(s74)*). The correlation coefficient r between the flex and position from the head has the following values. For forward motion: $r = -0.97$ ($p = 0.000$) for wild type; $r = -0.86$ ($p = 0.001$) for *unc-25(e156)*; $r = -0.83$ ($p = 0.002$) for *unc-68(r1158)*; $r = -0.71$ ($p = 0.014$) for *unc-54(s74)*. Similarly, for the backward motion: $r = -0.89$ ($p = 0.000$) for wild type; $r = -0.62$ ($p = 0.042$) for *unc-25(e156)*; $r = -0.72$ ($p = 0.013$) for *unc-68(r1158)*; $r = 0.41$ ($p = 0.208$) for *unc-54(s74)*. In all cases but one (for *unc-54* the backward motion r is positive but not significant) correlation are strong and negative, which implies that there is a significant decreasing trend of flex with position along the body. The line convention is the same as in (A), (B). Here and in other figures the worm's head position corresponds to the point 1 on the horizontal axis and its tail position to the point 11. The error bars in all figures are population standard deviations.

Fig. 4

Locomotion characteristics of the mutants with affected non-neuronal functions and wild-type *C. elegans* (forward motion). (A) Spatial distribution of the frequency of undulations for cuticle mutants *sqt-1(sc101)* (dashed line (red on-line), $N = 13$) and BE109 (dashed-dotted line (green on-line), $N = 9$), and wild-type (solid line (blue on-line), $N = 62$) worms. The error bars are population standard deviations. (B) Snapshots of worm postures: (a) wild type, (b) BE109, (c) *sqt-1(sc101)*, (d) *unc-54(s95)*. All of the mutants move on average slower than wild type, but their body posture and locomotory pattern can be either similar to wild type (panel (c)) or significantly different (panels (b) and (d)).

Fig. 5

Experimental non-monotonic (biphasic) dependence of the undulatory frequency on synaptic GABA signaling (forward motion). (A) Loss-of-function GABA mutants *unc-25(e156)* (dashed red line, $N = 4$), *unc-46(e177)* (dashed-dotted green line, $N = 4$), and *unc-18(e81); cho-1::unc-18::yfp* (dotted black line, $N = 14$) move with significantly lower frequencies than wild type (solid blue line) (non-parametric sign test for paired average frequencies along the body, $p < 0.05$). (B) Mutants *slo-1(js118); Pacr-2::slo-1* (dashed-dotted black lines representing 4 independent lines A, B, C, D) with increased GABA signaling and presumably wild-type levels of acetylcholine signaling move with significantly lower frequencies than wild type (solid blue line) (sign test, $p < 0.05$). (C) Similar to panel B: mutants *slo-1(js118); Pacr-2::slo-1* (dashed-dotted black line) are also slower than two types of animals with presumably recovered wild-type neu-

rotransmission in both GABA and cholinergic neurons: *slo-1(js118); Pacr-2::slo-1; Punc-25::slo-1* (solid red line, $N = 21$) and *slo-1(js118); Psnb-1::slo-1* (solid green line, $N = 20$) (sign test, $p < 0.05$).

Fig. 6

Experimental dependence of the undulatory frequency on synaptic acetylcholine signaling (forward motion). (A) In a background with elevated GABA signaling, *slo-1(js118); Pacr-2::slo-1* worms with presumably wild-type levels of acetylcholine move with either slightly higher (lines A ($N = 19$) and B ($N = 18$); dashed red line) or slightly lower (lines C ($N = 18$) and D ($N = 17$); dashed green line) frequencies than the control *slo-1(js118); Pacr-2::gfp* (solid blue line, $N = 19$), which has both types of neurotransmission increased above the wild-type level. (B) Mutants with increased acetylcholine and presumably rescued GABA signaling towards wild-type level, i.e., *slo-1(js118); Punc-25::slo-1* (dashed red line; $N = 18$ (line A), $N = 16$ (line B)), *slo-1(js118); Punc-17::slo-1* (dashed-dotted green line; $N = 16$ (line A), $N = 18$ (line B), $N = 18$ (line C)), and *slo-1(js118); Pcho-1::slo-1* (dotted black line; $N = 18$ (line A), $N = 18$ (line B), $N = 17$ (line C)), have slightly lower frequencies that the wild-type worms (solid blue line) (nonparametric sign-test for paired average frequencies along the body, $p < 0.05$).

Fig. 7

Oscillations generated in the circuit. (A) Model A. Upper panel: ventral muscle activities along the circuit (head M_{hv} - solid line (blue on-line), M_{v3} - dashed line (red on-line), M_{v6} - dashed-dotted line (green on-line)). Middle panel: corresponding dorsal muscle activities (M_{hd}, M_{d3}, M_{d6}) along the circuit. Note alternate corresponding os-

cillations in both these panels ($q_{ex} = 4.0$, $q_{in} = 3.0$). Lower panel: damped oscillations along the circuit (the same line convention as in the upper panel). For more posterior circuit elements oscillations become unstable only after a few cycles when either global excitation and inhibition are too small or muscle gap-junction coupling is too small ($q_{ex} = 2.0$, $q_{in} = 1.0$). This damping effect may explain the experimentally observed weak spatial decay of frequency for neuronal mutants with weak synaptic couplings (Suppl. Tables T1, T2). (B) The same for model B. (C) Oscillations in the circuit elements of model A. Upper panel: activities of head ventral X (solid line (blue on-line)) and Z (dashed line (red on-line)) neurons. Middle panel: activities of two interneurons AVB (solid line (blue on-line)) and PVC (dashed line (red on-line)). Note weak high frequency oscillations in both interneurons in contrast to other elements in the circuit. Lower panel: activities of ventral body wall motor neurons (no 2) excitatory (solid line (blue on-line)) and inhibitory (dashed line (red on-line)), and stretch receptors (dashed-dotted line (green on-line)) ($q_{ex} = 3.0$, $q_{in} = 2.0$). Note that almost all elements in the circuit oscillate with the same collective frequency, except the two interneurons, which exhibit weak high frequency oscillations (for some model parameters these oscillations are practically invisible). (D) The same for model B.

Fig. 8

Neuromuscular wave generated in the circuit. The wave propagates either towards the tail (A) for posteriorly directed stretch receptor coupling, or towards the head (B) for anteriorly directed coupling. The former corresponds to the forward motion circuit, whereas the latter to the backward motion circuit. Wave does not propagate

when a unidirectional stretch receptor feedback coupling is absent. (C) The phase lag of neighboring muscle activities is to a large extent both position and frequency independent. Also the phase lag between the head and the tail is essentially frequency independent: $0.97\times(2\pi)$ for 0.70 Hz, $1.03\times(2\pi)$ for 0.57 Hz, and $0.91\times(2\pi)$ for 0.46 Hz, which suggests frequency independence of the wavelength. Solid line (blue on-line) with diamonds corresponds to the frequency 0.70 Hz, dashed line (red on-line) with circles to 0.57 Hz, and dashed-dotted line (green on-line) with crosses to 0.46 Hz. (D) The phase lag of intermuscle activities (between no. 3 and 2) decreases with increasing the stretch receptor feedback coupling, although weakly if the coupling is sufficiently strong for both models A (solid line (blue on-line)) and B (dashed line (red on-line)). Parameters used in (A) and (B): $q_{ex} = 4.0$, $q_{in} = 2.0$, and $g_m = 0.4$ (model A). Parameters used in (C) (model B only) and (D) (both models): $q_{ex} = 3.0$, $q_{in} = 2.0$.

Fig. 9

Theoretical dependence of the frequency of oscillations in the circuit on the global synaptic inhibition q_{in} (A, B) and global synaptic excitation q_{ex} (C, D). Both models A and B give a qualitatively similar biphasic dependence of frequency on inhibition and excitation. (A), (B) For very weak inhibition oscillations are unstable. (C), (D) For both too weak and too strong excitation oscillations are unstable. (A), (B) The solid line (blue on-line) corresponds to $q_{ex} = 4.0$ and dashed line (red on-line) to $q_{ex} = 2.0$. (C), (D) The solid line (blue on-line) corresponds to $q_{in} = 5.0$ and dashed line (red on-line) to $q_{in} = 1.0$. These biphasic relationships can be explained by the changes in temporal characteristics of muscle voltage in response to changes in the levels of

inhibition (E) and excitation (F). Parameters used: (E) $q_{ex} = 4.0$ and $q_{in} = 0.5$ (upper panel), $q_{in} = 4.5$ (middle panel), $q_{in} = 35.0$ (lower panel) in model B; (F) $q_{in} = 5.0$ and $q_{ex} = 1.2$ (upper panel), $q_{in} = 3.8$ (middle panel), $q_{in} = 6.6$ (lower panel) in model A.

Fig. 10

Theoretical dependence of the frequency of oscillations in the circuit on the muscle characteristics. Models A and B give qualitatively similar behaviors of frequency on muscle gap junction coupling g_m (A, B) and muscle calcium signaling strength w_{mm} (C, D). (A), (B) Monotonic increase of frequency with increasing gap junction coupling. Solid line (blue on-line) corresponds to $q_{ex} = 2.0$, $q_{in} = 2.0$ and dashed line (red on-line) to $q_{ex} = 2.0$, $q_{in} = 4.0$. (C), (D) Biphasic or triphasic dependence on frequency on calcium signaling. The curve's shape depends on a relative strengths of the global excitation and inhibition. For very large calcium signaling levels oscillations in the circuit become unstable. Solid line (blue on-line) corresponds to $q_{ex} = 4.0$, $q_{in} = 4.0$ and dashed line (red on-line) to $q_{ex} = 1.5$, $q_{in} = 7.0$.

Fig. 11

Theoretical dependence of the frequency of oscillations in the circuit on the stretch receptor coupling parameter w_{es}. The behavior of model A (A) differs from model B (B) only in the weak coupling regime. In this regime oscillations in model B are unstable, while model A shows unmodulated high frequency oscillations of head interneurons. In both figures, the solid line (blue on-line) corresponds to $q_{ex} = 2.0$, $q_{in} = 2.0$ and the dashed line (red on-line) to $q_{ex} = 4.0$, $q_{in} = 1.0$.

Fig. 12

Theoretical dependence of the frequency of oscillations on the muscle and stretch receptor time constants. (A) Decrease of the oscillatory frequency with increasing the muscle membrane time constant τ_m in model A (solid line (blue on-line)) and model B (dashed line (red on-line)). (B) Decrease of the oscillatory frequency with increasing the stretch receptor time constant τ_s in model A (solid line (blue on-line)) and model B (dashed line (red on-line)). Note that the frequency is much larger in model B for small values of τ_m and τ_s. In both figures, we used $q_{ex} = 3.0$ and $q_{in} = 2.0$

Figure 1

A

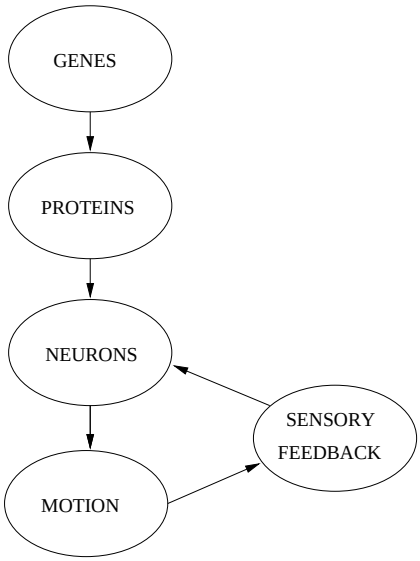

B

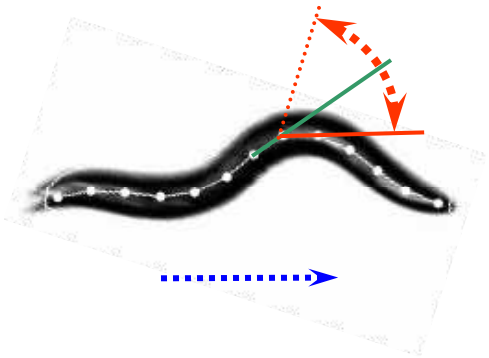

A

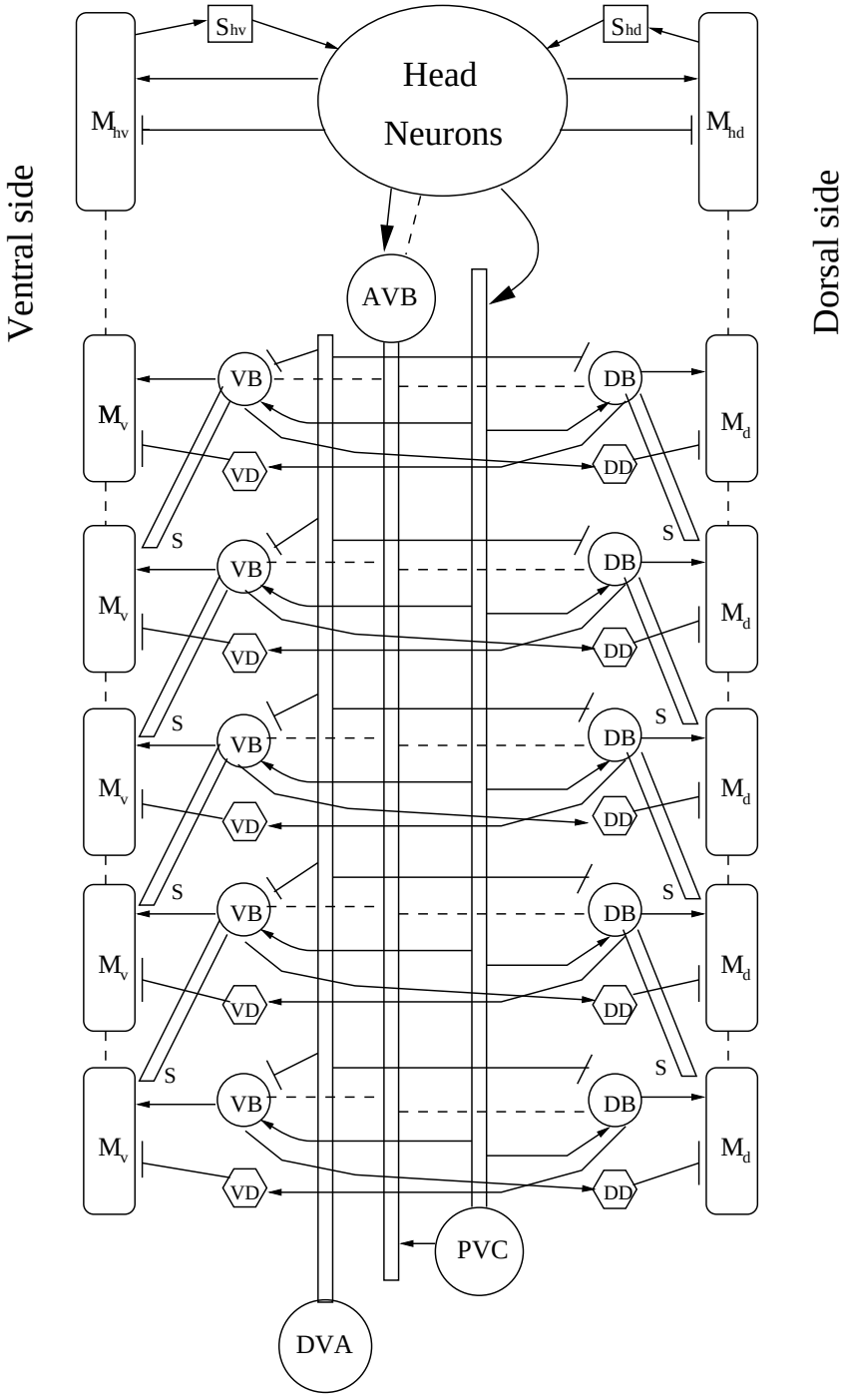
Ventral side
Dorsal side
Head
Neurons
AVB
PVC
DVA
VB
DB
VD
DD
S

B

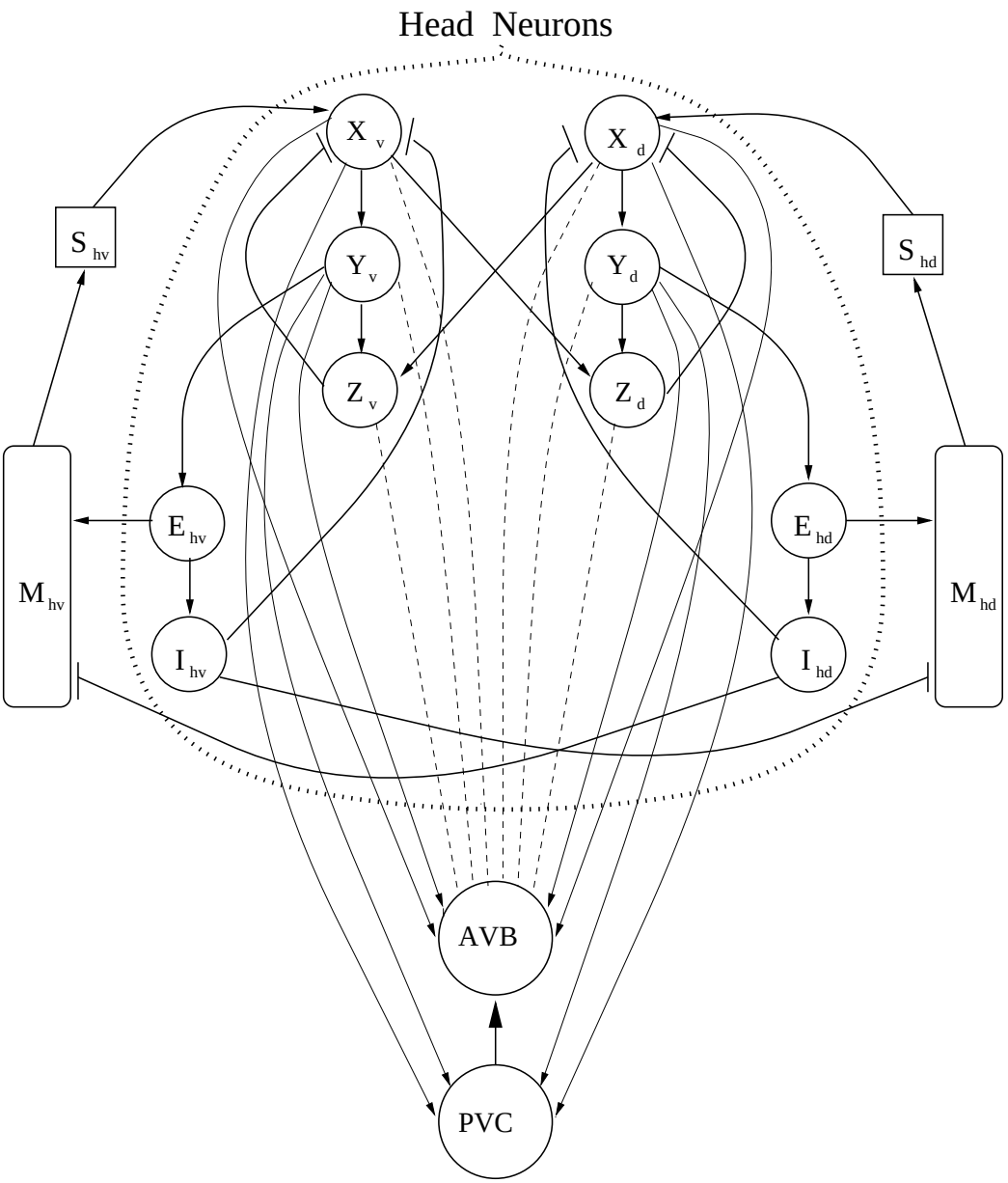
Head Neurons
X v
X d
S hv
S hd
Y v
Y d
Z v
Z d
E hv
E hd
M hv
M hd
I hv
I hd
AVB
PVC

Figure 2

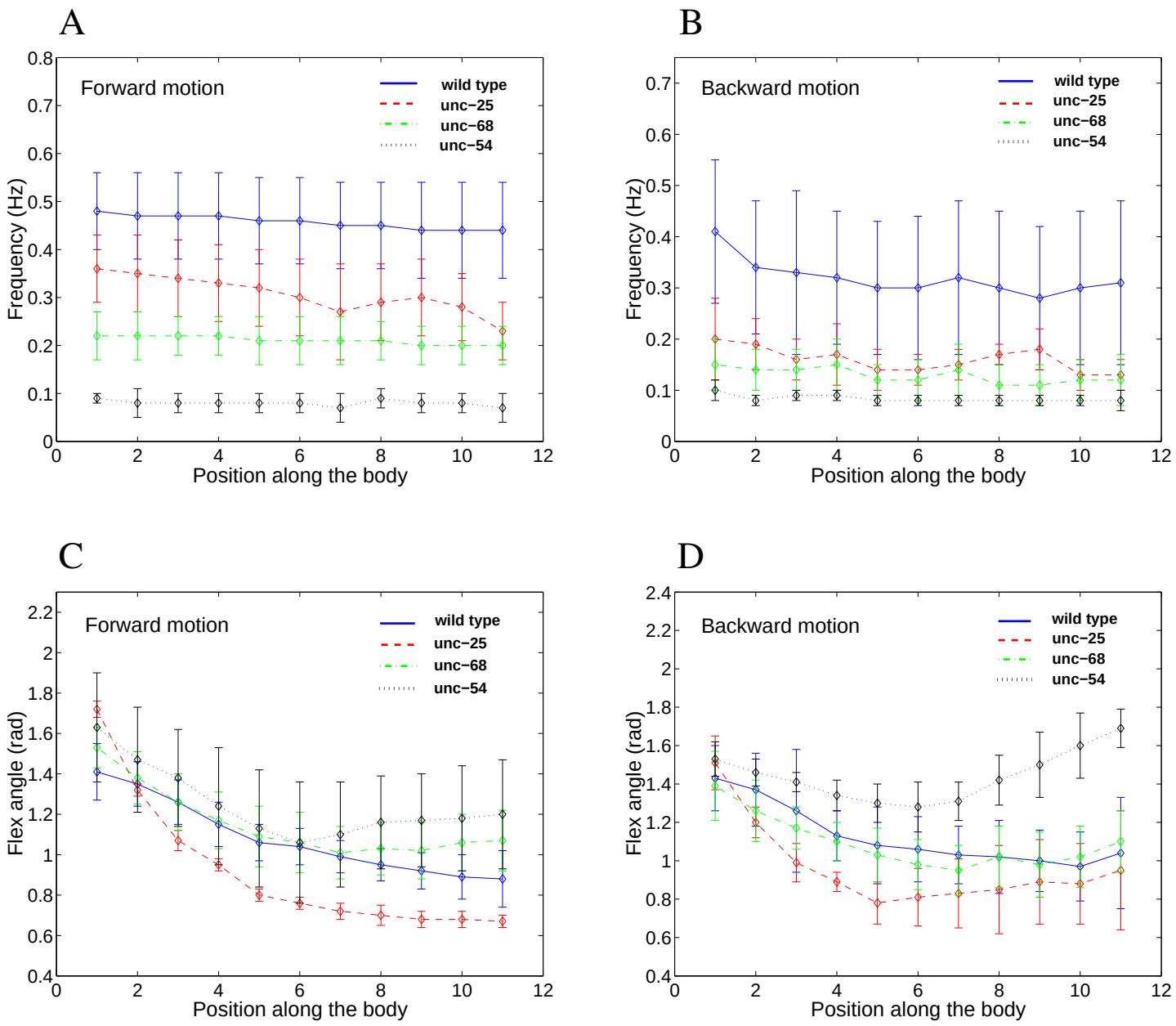
A
Forward motion
wild type
unc−25
unc−68
unc−54
Frequency (Hz)
Position along the body
B
Backward motion
wild type
unc−25
unc−68
unc−54
Frequency (Hz)
Position along the body
C
Forward motion
wild type
unc−25
unc−68
unc−54
Flex angle (rad)
Position along the body
D
Backward motion
wild type
unc−25
unc−68
unc−54
Flex angle (rad)
Position along the body

Figure 3

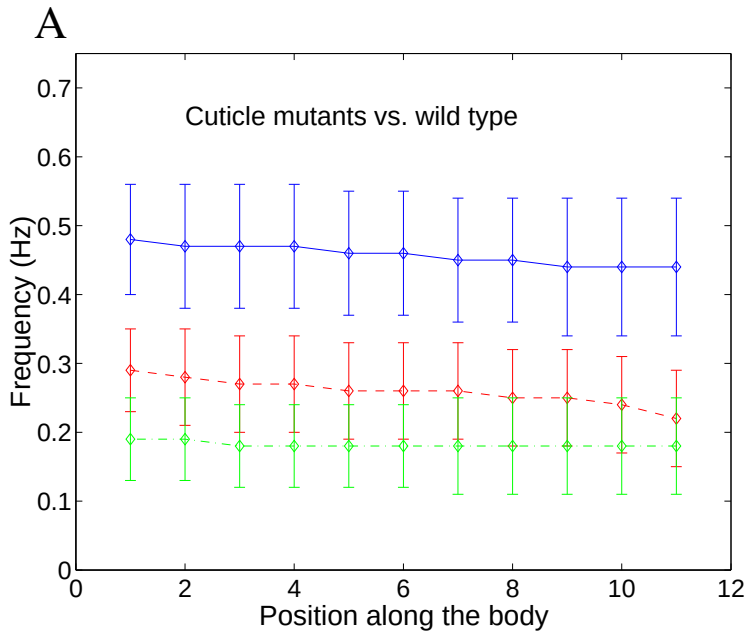
A
Cuticle mutants vs. wild type
Frequency (Hz)
Position along the body
0
0.1
0.2
0.3
0.4
0.5
0.6
0.7
0
2
4
6
8
10
12

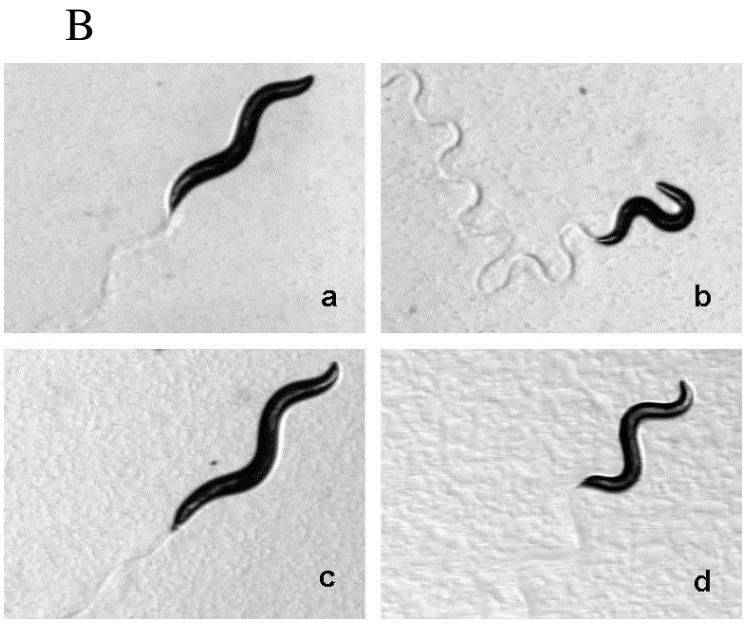
B
a
b
c
d

Figure 4

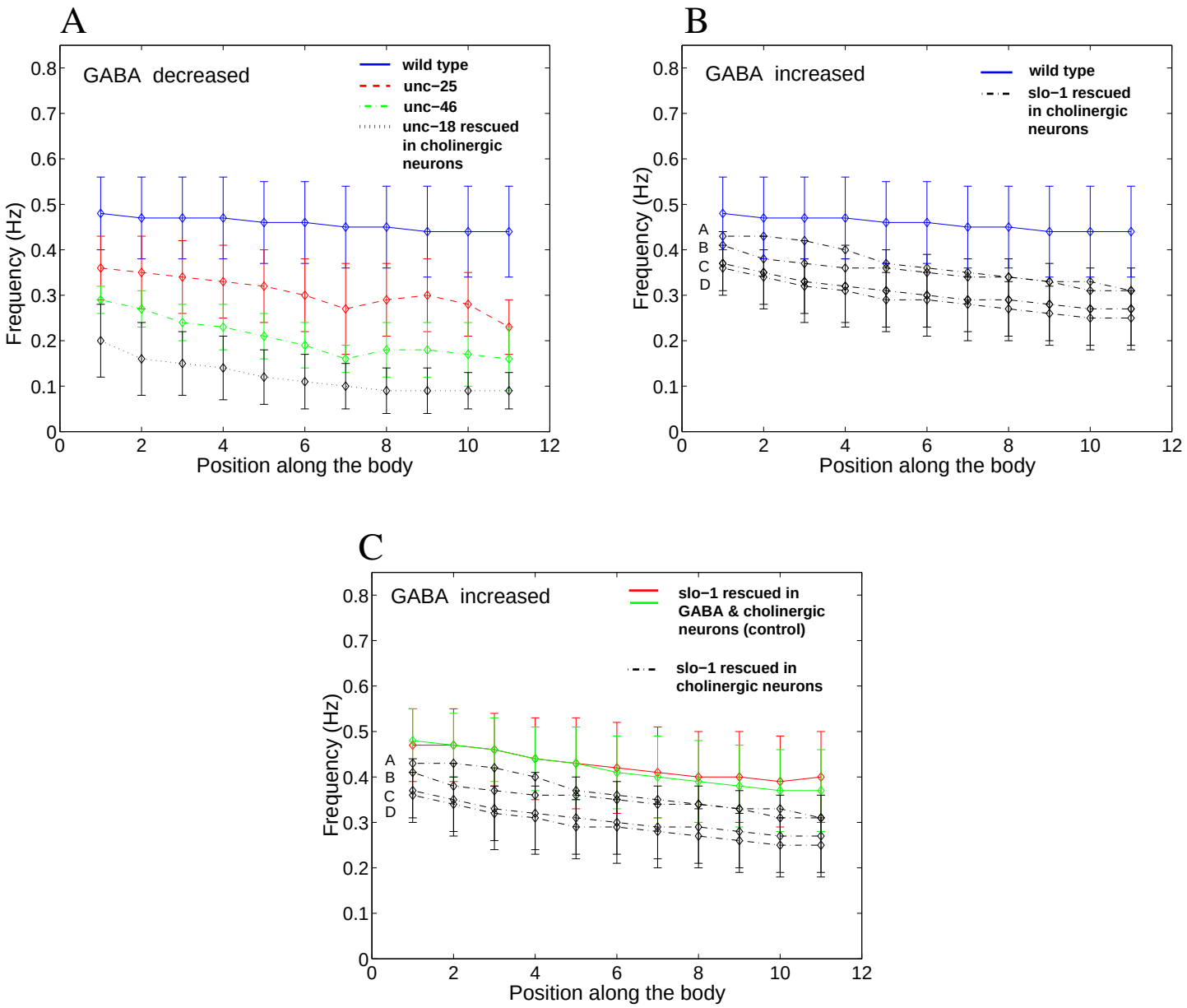
A
GABA decreased
wild type
unc−25
unc−46
unc−18 rescued in cholinergic neurons
Frequency (Hz)
Position along the body
B
GABA increased
wild type
slo−1 rescued in cholinergic neurons
A
B
C
D
Frequency (Hz)
Position along the body
C
GABA increased
slo−1 rescued in GABA & cholinergic neurons (control)
slo−1 rescued in cholinergic neurons
A
B
C
D
Frequency (Hz)
Position along the body

Figure 5

A

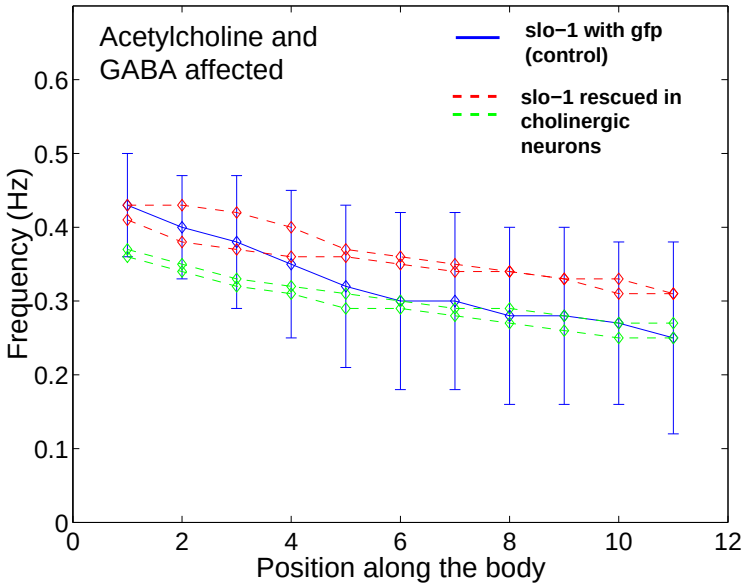
Acetylcholine and
GABA affected
slo−1 with gfp
(control)
slo−1 rescued in
cholinergic
neurons
Frequency (Hz)
Position along the body
0
0.1
0.2
0.3
0.4
0.5
0.6
0
2
4
6
8
10
12

B

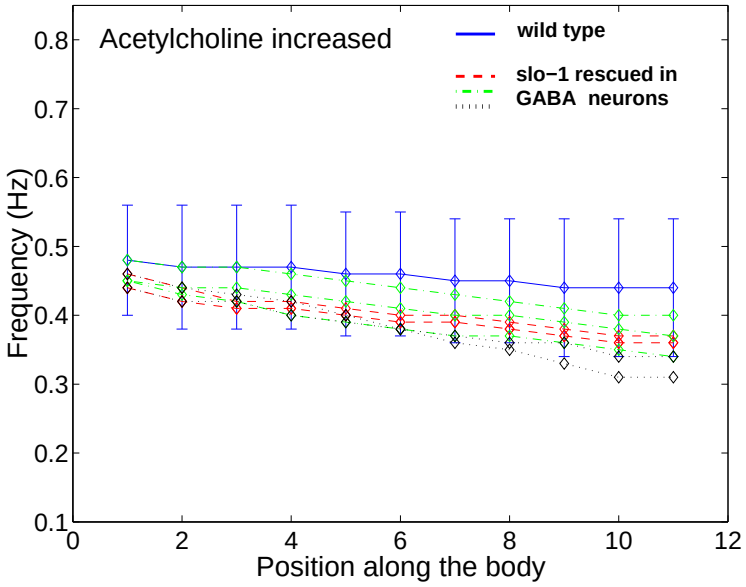
Acetylcholine increased
wild type
slo−1 rescued in
GABA neurons
Frequency (Hz)
Position along the body
0.1
0.2
0.3
0.4
0.5
0.6
0.7
0.8
0
2
4
6
8
10
12

Figure 6

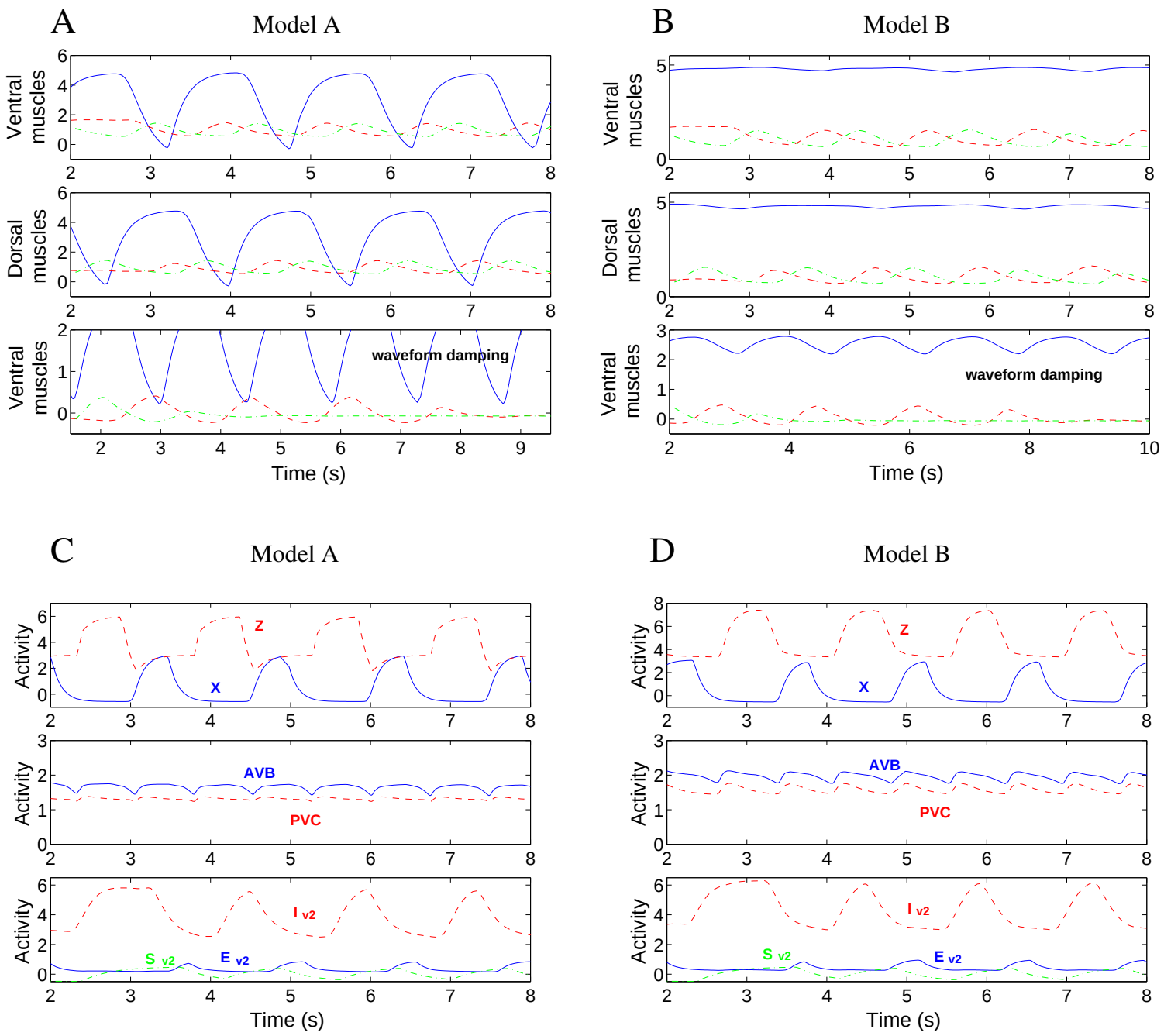
A
Model A
Ventral muscles
Dorsal muscles
Ventral muscles
waveform damping
Time (s)
B
Model B
Ventral muscles
Dorsal muscles
Ventral muscles
waveform damping
Time (s)
C
Model A
Activity
Z
X
AVB
PVC
I v2
S v2
E v2
Time (s)
D
Model B
Activity
Z
X
AVB
PVC
I v2
S v2
E v2
Time (s)

Figure 7

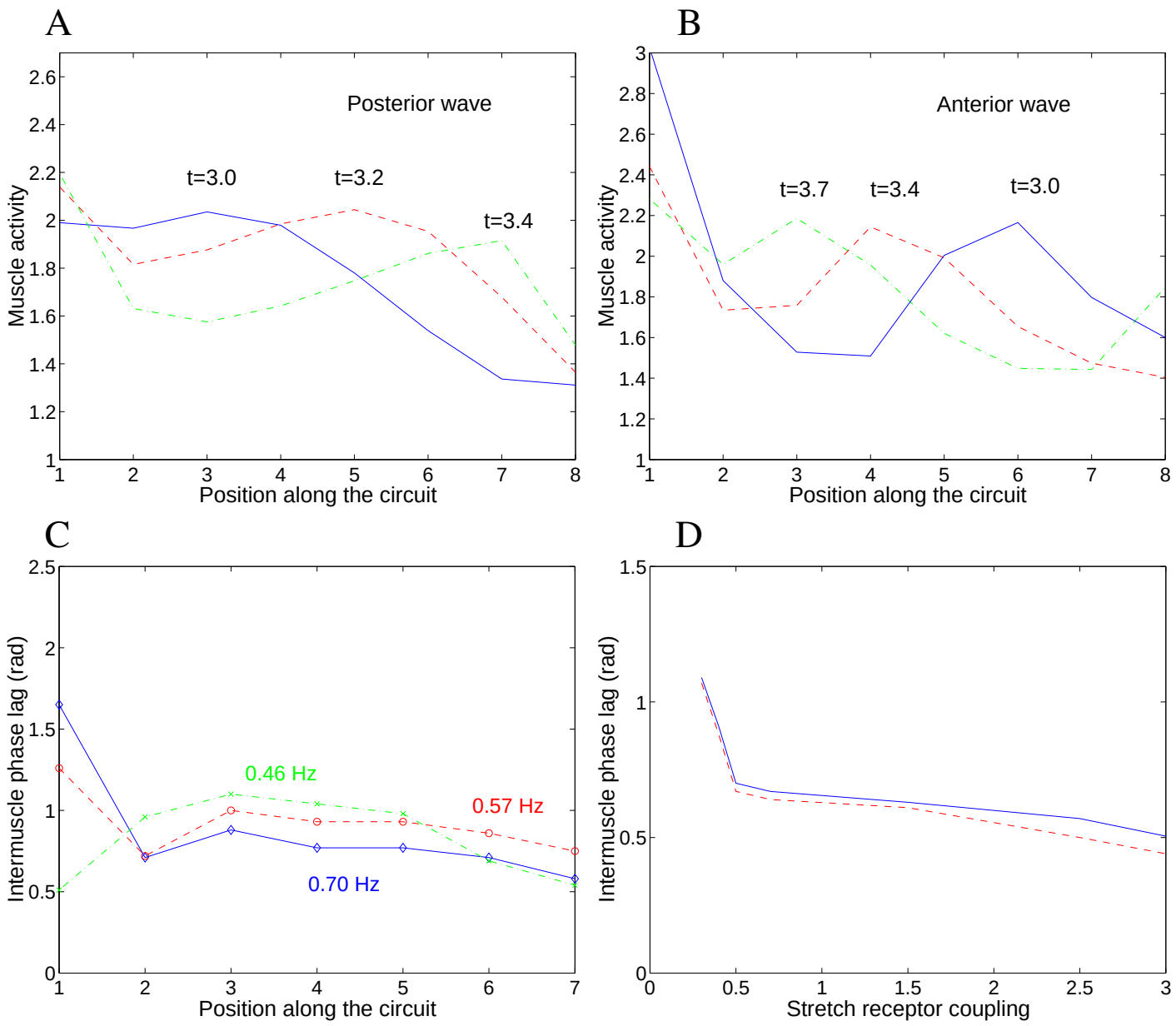
A
Posterior wave
t=3.0
t=3.2
t=3.4
Muscle activity
Position along the circuit
B
Anterior wave
t=3.7
t=3.4
t=3.0
Muscle activity
Position along the circuit
C
0.46 Hz
0.57 Hz
0.70 Hz
Intermuscle phase lag (rad)
Position along the circuit
D
Intermuscle phase lag (rad)
Stretch receptor coupling

Figure 8

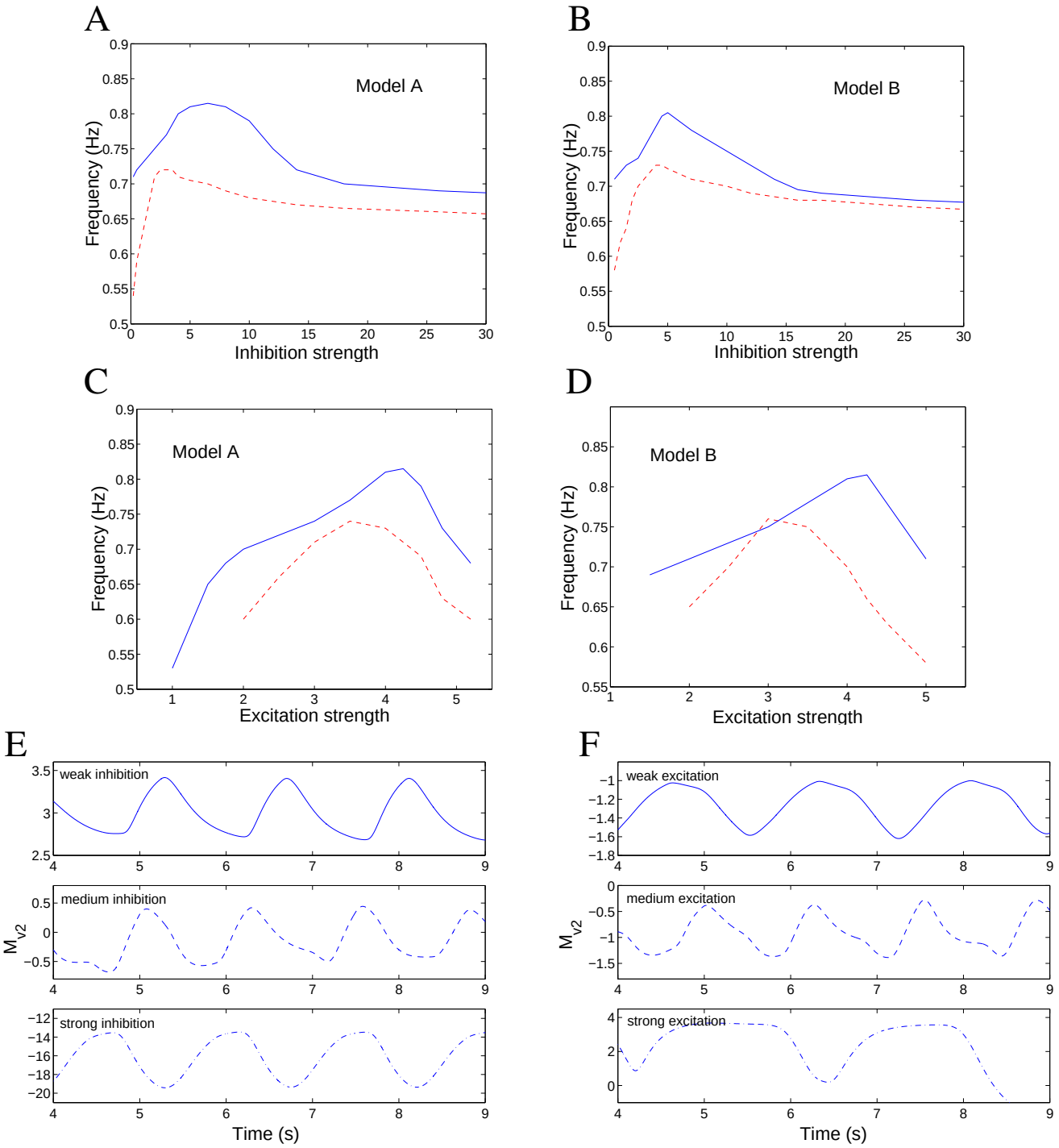
A
Model A
Frequency (Hz)
Inhibition strength
B
Model B
Frequency (Hz)
Inhibition strength
C
Model A
Frequency (Hz)
Excitation strength
D
Model B
Frequency (Hz)
Excitation strength
E
weak inhibition
medium inhibition
strong inhibition
M_{v2}
Time (s)
F
weak excitation
medium excitation
strong excitation
M_{v2}
Time (s)

Figure 9

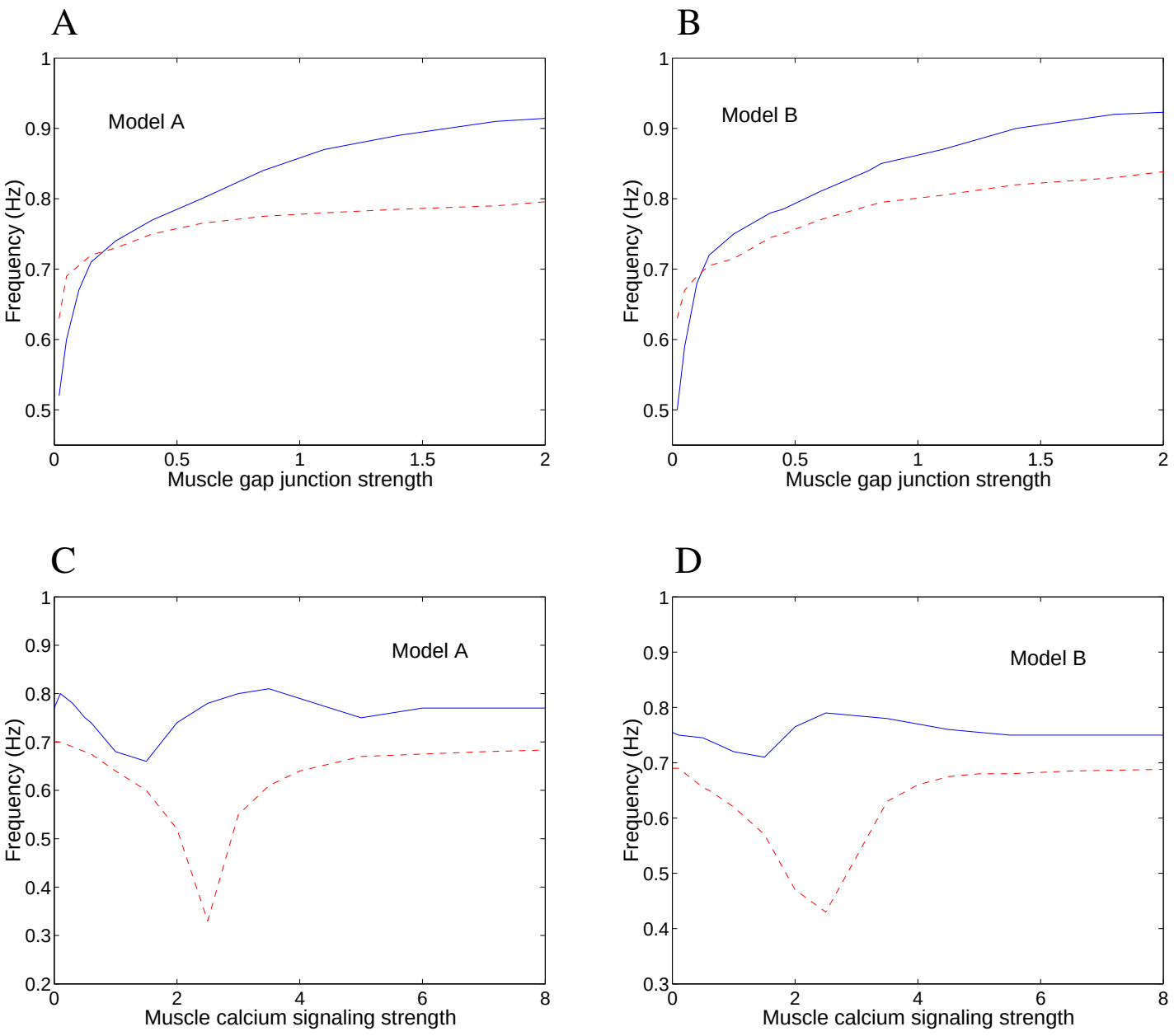
A
Model A
Frequency (Hz)
Muscle gap junction strength
B
Model B
Frequency (Hz)
Muscle gap junction strength
C
Model A
Frequency (Hz)
Muscle calcium signaling strength
D
Model B
Frequency (Hz)
Muscle calcium signaling strength

Figure 10

A

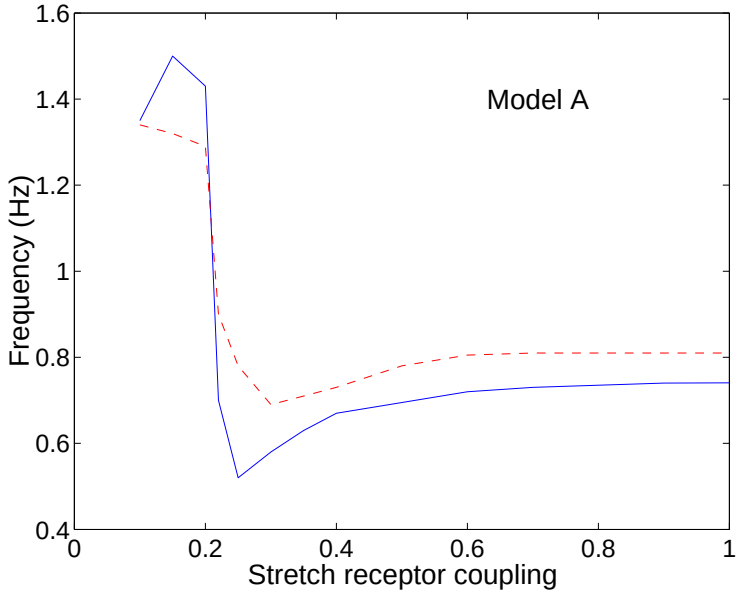
Model A
Frequency (Hz)
Stretch receptor coupling
1.6
1.4
1.2
1
0.8
0.6
0.4
0
0.2
0.4
0.6
0.8
1

B

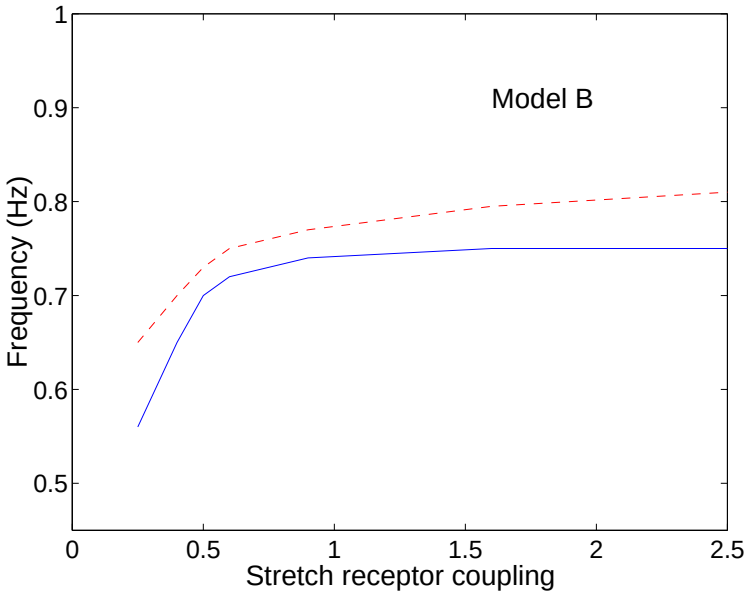
Model B
Frequency (Hz)
Stretch receptor coupling
1
0.9
0.8
0.7
0.6
0.5
0
0.5
1
1.5
2
2.5

Figure 11

A

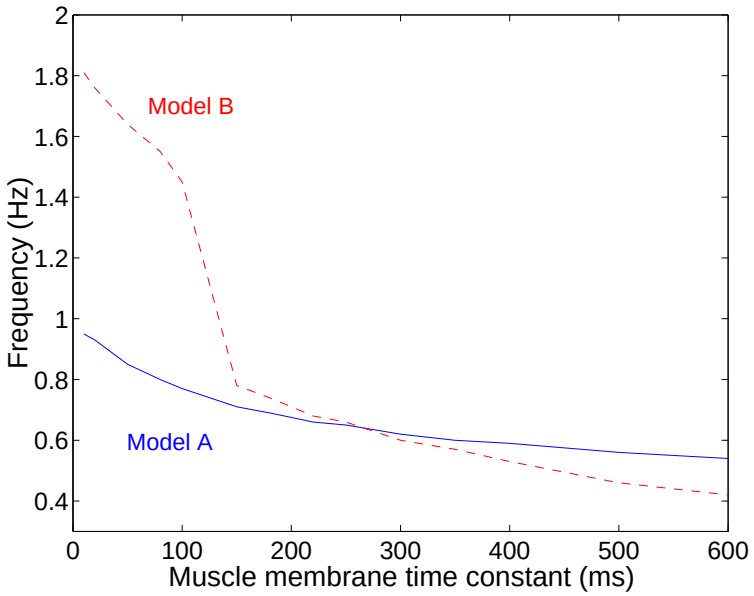
Model B
Model A
Frequency (Hz)
Muscle membrane time constant (ms)
2
1.8
1.6
1.4
1.2
1
0.8
0.6
0.4
0
100
200
300
400
500
600

B

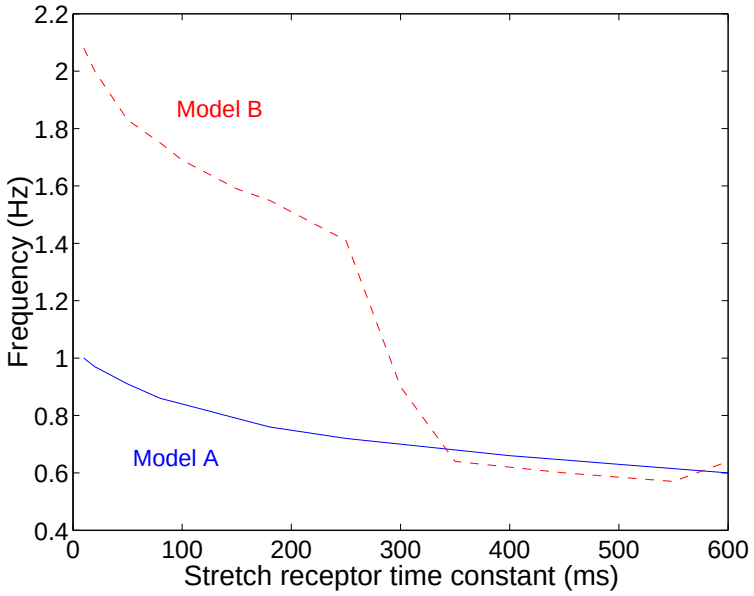
Model B
Model A
Frequency (Hz)
Stretch receptor time constant (ms)
2.2
2
1.8
1.6
1.4
1.2
1
0.8
0.6
0.4
0
100
200
300
400
500
600

Figure 12